

Model-Based Calibration and Control of Tailpipe Nitrogen Oxide Emissions in a Light-Duty Diesel Engine and Its Assessment through Model-In-The-Loop

*Original*

Model-Based Calibration and Control of Tailpipe Nitrogen Oxide Emissions in a Light-Duty Diesel Engine and Its Assessment through Model-In-The-Loop / D'Ambrosio, Stefano; DI DIO, Cosimo; Finesso, Roberto. - In: ENERGIES. - ISSN 1996-1073. - ELETTRONICO. - 16:24(2023), pp. 1-29. [10.3390/en16248030]

*Availability:*

This version is available at: 11583/2984670 since: 2023-12-21T19:03:08Z

*Publisher:*

MDPI

*Published*

DOI:10.3390/en16248030

*Terms of use:*

This article is made available under terms and conditions as specified in the corresponding bibliographic description in the repository

*Publisher copyright*

(Article begins on next page)



*energies*



Article

---

# Model-Based Calibration and Control of Tailpipe Nitrogen Oxide Emissions in a Light-Duty Diesel Engine and Its Assessment through Model-In-The-Loop

---

Stefano d'Ambrosio, Cosimo di Dio and Roberto Finesso

Special Issue

Vehicle Engines and Powertrains: Performance, Combustion and Emission

Edited by




Dr. Roberto Finesso and Dr. Omar Marelo



<https://doi.org/10.3390/en16248030>

## Article

# Model-Based Calibration and Control of Tailpipe Nitrogen Oxide Emissions in a Light-Duty Diesel Engine and Its Assessment through Model-In-The-Loop

Stefano d'Ambrosio , Cosimo di Dio  and Roberto Finesso \* 

Energy Department, Politecnico di Torino, Corso Duca degli Abruzzi 24, 10129 Torino, Italy; stefano.dambrosio@polito.it (S.d.); cosimo.didio@polito.it (C.d.D.)

\* Correspondence: roberto.finesso@polito.it; Tel.: +39-011-090-4493

**Abstract:** The present paper investigates two different strategies for model-based calibration and control of tailpipe nitrogen oxide emissions in a light-duty 3.0 L diesel engine equipped with an aftertreatment system (ATS). The latter includes a diesel oxidation catalyst (DOC), a diesel particulate filter (DPF), and an underfloor selective catalytic reduction (SCR) device, in which the injection of diesel exhaust fluid (DEF), marketed as 'AdBlue', is also taken into account. The engine was modeled in the GT-SUITE environment, and a previously developed model-based combustion controller was integrated in the model, which is capable of adjusting the start of injection of the main pulse and the total injected fuel mass, in order to achieve desired targets of engine-out nitrogen oxide emissions (NO<sub>x</sub>) and brake mean effective pressure (BMEP). First, a model-based calibration strategy consisting of the minimization of an objective function that takes into account fuel consumption and AdBlue injection was developed and assessed by exploring different weight factors. Then, a direct model-based controller of tailpipe nitrogen oxide emissions was designed, which exploits the real-time value of the SCR efficiency to define engine-out NO<sub>x</sub> emission targets for the combustion controller. Both strategies exploit the model-based combustion controller and were tested through a Model-in-the-Loop (MiL) under steady-state and transient conditions. The advantages in terms of tailpipe NO<sub>x</sub> emissions, fuel consumption, and AdBlue injection were finally discussed.

**Keywords:** diesel engines; tailpipe nitrogen oxides; SCR; model-based calibration; Model-in-the-Loop



**Citation:** d'Ambrosio, S.; di Dio, C.; Finesso, R. Model-Based Calibration and Control of Tailpipe Nitrogen Oxide Emissions in a Light-Duty Diesel Engine and Its Assessment through Model-In-The-Loop. *Energies* **2023**, *16*, 8030. <https://doi.org/10.3390/en16248030>

Academic Editor: Xiaohuan Zhao

Received: 31 October 2023

Revised: 1 December 2023

Accepted: 8 December 2023

Published: 12 December 2023



**Copyright:** © 2023 by the authors. Licensee MDPI, Basel, Switzerland. This article is an open access article distributed under the terms and conditions of the Creative Commons Attribution (CC BY) license (<https://creativecommons.org/licenses/by/4.0/>).

## 1. Introduction

Vehicle emission standards concerning pollutant and CO<sub>2</sub> levels have become more and more stringent in the last few years. For example, Euro6d-Temp emission regulations are currently adopted in Europe, and the European Union (EU) will approve the new Euro7 limits. Additionally, the EU is also aiming to achieve future targets for CO<sub>2</sub> emission limits from cars and heavy-duty vehicles in upcoming decades. The 'Fit-for-55' package proposes a target of zero tailpipe CO<sub>2</sub> emissions from newly sold cars and light-duty commercial vehicles starting in 2035 [1]. Moreover, a proposal is currently under discussion to achieve a target of 90% fleet-average reduction in tailpipe CO<sub>2</sub> emissions from heavy-duty trucks and long-distance buses, with respect to 2019, starting from 2040 [2]. If these measures are confirmed, future vehicles in the EU will have to be propelled by full-electric powertrains or hydrogen-fueled powertrains (including fuel cells and internal combustion engines (ICEs)). Some exceptions may be related to vehicles equipped with ICEs fueled with e-fuels, as reported by recent proposals [3]. Concerning fully electric vehicles (EVs), however, several problems still have to be addressed before they can replace conventional vehicles equipped with thermal powertrains without penalizing users' driving experience. The first issue is related to the limited driving range of EVs, which is currently, on average, of the order of 359 km when considering the vehicles available in the market [4]. This limited driving range penalizes the user, especially when considering long travels over

extra-urban scenarios. Another issue is related to the long charging times, which may lead to long queues at charging stations [5]; this is also due to a lack of charging infrastructure. Regarding required charging times, even when considering fast chargers (60 kW) instead of conventional Level 1 chargers (1.8 kW), a recharging time of 20 min is still required to deliver an average driving range of 95–130 km [6]. Moreover, fast charging can also be associated with an acceleration in battery degradation of around 20% [6] with a related increase in the user total cost of ownership, and it brings more safety issues than Level 1 charging. Another drawback of the extended use of EVs is the higher electric power demands that are required, especially in residential areas, because of home car charging, with possible issues related to safety and the power grid's ability to maintain a stable voltage [7]. EVs are also characterized by higher initial costs with respect to vehicles equipped with thermal engines, making it necessary for governments to offer incentive policies. Finally, the environmental and energy impacts of EVs depend on the electric energy production source to a great extent [8].

Concerning vehicles fueled with hydrogen, the main issues are related to the lack of infrastructure for hydrogen supply, to the high hydrogen production price, to the difficult hydrogen storage (which requires pressure levels of several hundreds of bar), to the risk of explosion, and to the very high vehicle costs. A recent comparison between EVs and hydrogen-fueled vehicles [9] suggests that the use of hydrogen-fueled vehicles could be complementary to that of EVs, especially for low-temperature scenarios and heavy-duty applications.

Based on the previous background, in the authors' opinion, powertrains equipped with ICEs will still play a major role over the next decades, especially concerning heavy-duty applications, and therefore, research efforts for reducing their environmental impact in terms of pollutant and CO<sub>2</sub> emissions are still needed.

Different techniques have been introduced in the last years to reduce the environmental impact of ICEs, such as downsizing [10], alternative fuels [11], advanced combustion and injection systems [12], fuel thermal management [13], sensor-based control algorithms [14], model-based control algorithms [15–26], and the recovery of thermal energy [27].

Among the previous techniques, model-based control algorithms are playing a significant role due to the increasingly high performance of vehicle control units and the possibility of integration with model-based energy management systems. This can be confirmed by recent research projects, such as the IMPERIUM H2020 one [15], which was aimed at achieving a reduction in AdBlue and fuel consumption of up to 20% in heavy-duty trucks through the adoption of a model-based vehicle energy management supervisor. Within that project, the authors developed a model-based combustion controller capable of achieving desired targets of torque and engine-out NO<sub>x</sub> emissions in real-time.

It is clear that these algorithms require accurate modeling of the whole engine or of specific engine subsystems, and this task can be carried out according to several degrees of detail. In general, two categories of engine models can be identified, i.e., physics-based models and black-box models.

Physics-based models rely on the resolution of fundamental physical equations, i.e., conservation of mass and energy [28], while black-box models typically include artificial intelligence systems, such as artificial neural networks, and require extended experimental datasets for training [29]. With reference to the first family of models, several approaches with different degrees of detail can be identified, i.e., 3D-CFD (computational fluid dynamics) models, 1D-CFD models and mean-value 0D models. Models based on 3D-CFD rely on the numerical solution of the three-dimensional Navier–Stokes equations and provide a detailed description of the fluid dynamics evolution inside the engine, but they require a very long computational time. Therefore, they are typically adopted to simulate specific engine subsystems, such as the combustion chamber, the intake/exhaust pipes, or the ATS system. An example is provided in [30], in which the authors study a flamelet progress variable approach for simulating a reacting diesel spray using a 3D-CFD methodology. Models based on 1D-CFD are instead capable of providing the fluid-dynamic evolution

along one selected direction, and are commonly adopted in codes which are capable of simulating the entire engine, with a reasonable computational time. Thus, they can be used for such applications as virtual engine design, calibration or Model-in-the-Loop, such as the example provided in [31]. However, they cannot be used as fast simulation tools to be embedded in model-based controllers. Mean value 0D models are instead more suitable for this purpose, since they are characterized by shorter computational times than 1D-CFD models, but they are still able to provide a good predictive capability at steady-state and transient conditions [32]. Zero-dimensional models are not capable of providing a detailed fluid dynamics analysis of the system but are based on physically consistent equations to model the different engine components, including the combustion and emission formation processes. For example, in [14,15] the authors exploit a mean-value real-time physics-based model to realize torque and engine-out NO<sub>x</sub> controllers for 3.0 L and 11.0 L diesel engines, respectively. The study in [33] reports instead a zero-dimensional mixing controlled combustion model for a marine diesel engine, while a fast physics-based NO<sub>x</sub> emission model is proposed in [34].

The second category of models is based on the black-box approach. These models describe the input-output relation of a system through purely mathematical algorithms, without the need of describing and modeling the related physical processes. Artificial neural networks and support vector machines are typical examples of black-box methods. These algorithms are characterized by very-short computational time, thus they are suitable to be embedded in model-based controllers, but their training requires a higher number of experimental tests than mean-value physics-based models; moreover, they are less reliable outside the calibration range. Some examples of black-box models applied in the ICE field simulation are reported in [35–37].

From the previous analysis, it can be seen that mean-value physics-based models and black-box models are the most suitable approaches to realize model-based control algorithms, where the first family should be preferred when a large experimental dataset is not available for calibration.

Among the different model-based algorithms that have been developed in the ICE field in the last years, both in gasoline [17] and diesel engines [18–26], combustion controllers can offer a high potential for fuel consumption and pollutant formation reduction, especially when they are integrated with the ATS management system. In fact, this can allow us to define optimal sets of engine calibration parameters in real-time (such as injection timing and quantity), taking into account the actual efficiency of the ATS. An integrated approach for the combustion system and ATS management may lead to an improvement of the engine system behavior, compared with the conventional calibration methods, which are typically carried out separately for the combustion-related parameters and ATS-related parameters on the basis of engineering experience [18] and are based on traditional PID and control schemes. Several studies have recently been conducted on the development of integrated combustion/ATS control systems in diesel engines [18–26] which highlight that the related interest is still relevant. Pontryagin's minimum principle (PMP), equivalent consumption minimization strategy (ECMS), dynamic programming (DP), model predictive control (MPC), and combined systems are commonly adopted approaches for supervisory integrated powertrain control [19]. The DP algorithm is a global optimizer, which cannot be embedded onboard due to the high computational cost and is applied to derive the reference benchmark solution, while the other methods can be properly handled to realize real-time controllers. For example, study [18] presented a supervisory control strategy based on PMP which is able to simultaneously optimize the air/fuel path and ATS in a heavy-duty diesel engine. In that study, the optimizer required a simplified model of the system to be implemented, and the authors showed that the performance of the controller is similar to that of a global optimizer based on dynamic programming (DP).

An ECMS-based supervisory control strategy for a light-duty diesel engine with LNT/SCR is presented in [19], which is able to select different engine modes to minimize a cost function that takes into account fuel and AdBlue.

In [20], the authors performed a comparison between the performance of a dynamic programming-based optimizer, a conventional PMP-based optimizer and a real-time PMP-based optimizer for a heavy-duty engine equipped with ATS. In that study, the engine was modeled by a quasi-static approach, and it was shown that a real-time PMP-based optimizer is capable of providing a similar performance to that of the DP-based one.

In [21], a real-time implementable supervisor, based on the PMP is presented for a Euro VI diesel engine with an electrified waste heat recovery system.

The studies reported in [22,23] propose Equivalent Consumption Minimization Strategy (ECMS) based controllers for non-causal optimal control of SCR and air path of diesel engines. In particular, in [22] a back stepping based active NOx control is used together with a stationary optimization methodology, ignoring transients, while in [23] a model-based and integrated strategy for hybrid electric vehicle (HEV) power management and aftertreatment control with preview information of road grade is proposed. In [24], combined control of start of injection (SOI), EGR, and urea injection is performed using MPC. In [25,26], integrated approaches for engine and ATS management, which are based on MPC and exploit a steady-state model, are proposed for heavy-duty applications. However, as reported in [18], the latter methods may require high computational resources, such as those based on PMP, which make their implementation on an engine control unit (ECU) quite challenging.

For the sake of clarity, Table 1 reports a summary of the methodology and main results obtained in previous studies focused on similar topics to those reported in this paper, with additional details.

**Table 1.** Summary of the methodology and main results obtained in previous studies concerning supervisory control strategies for integrated diesel engine ATS management.

Reference	Developed Methodology	Main Results
Van Dooren et al. [18]	PMP based. Target: fuel and AdBlue minimization while satisfying tailpipe NOx target limits. Controlled variables: injection timing and EGR rate.	The performance is close to the globally optimal solution based on DP.
Velmurugan et al. [19]	ECMS based. Target: fuel and AdBlue minimization while satisfying tailpipe emission limits. Controlled variables: calibration maps corresponding to different engine modes	Overall fuel equivalent cost reduction around 0.6–1% with respect to the baseline engine.
Donkers et al. [20]	PMP based (conventional and real-time). Target: fuel and AdBlue costs minimization while satisfying tailpipe NOx target limits	Conventional PMP yields almost the same results as DP, and the real-time implementable controller only deviates approximately 0.08–0.16% from the optimal solution.
Feru et al. [21]	Simplified PMP based (real-time implementable version). Target: minimization of a weighted function that includes fuel consumption, AdBlue, and fuel consumption related to active DPF regeneration, while satisfying cumulative tailpipe NOx emission constraints. Control variables: EGR valve position, VGT position, internal battery power.	Within the tailpipe NOx limit, the proposed strategy shows an additional 3.5% CO <sub>2</sub> emission reduction while AdBlue dosage and particulate matter are reduced by 2.5% and 19%, respectively.
Chen et al. [22]	ECMS based. Backstepping-based active NOx control is used together with a stationary optimization methodology.	In comparison with a passive NOx control method, 5.86% of engine fuel consumption can be reduced without significantly penalizing the tailpipe NOx and ammonia emissions.

Table 1. Cont.

Reference	Developed Methodology	Main Results
Ma et al. [23]	ECMS based. Model-based and integrated strategy for hybrid electric vehicle (HEV) power management and aftertreatment control with preview information of road grade. Target: minimization of a cost function including cumulative NO <sub>x</sub> , NH <sub>3</sub> emissions, fuel, SOC deviation and vehicle velocity deviation.	The proposed control design provides a synergy among engine, motor, battery, aftertreatment system, and road condition to accomplish a minimal overall predefined cost.
Westerlund et al. [24]	MPC-based. Combined control of start of injection (SOI), EGR, urea injection is performed. Target: minimization of a cost function which is based on fuel consumption and equivalent urea cost.	Compared to a more conservative steady state calibration with NO <sub>x</sub> emissions on the same level, peak NH <sub>3</sub> slip is reduced from 153 to 46.9 ppm, and fuel consumption is improved with 1.5% in the hot-start WHTC.
Wassen et al. [25]	MPC based. The actuators are EGR valve, wastegate valve, intake throttle valve. Target: minimization of a weighted cost function that includes consumption of fuel and urea, while respecting selected limitations in terms of engine-out NO <sub>x</sub> and temperature.	Controller embedded in the ECU. The results show a significant reduction in tailpipe BSNO <sub>x</sub> with reduction in BSFC.
Karim et al. [26]	Nonlinear MPC-based strategy. Target: minimizing fuel and AdBlue consumption while fulfilling NO <sub>x</sub> emission limits. The supervisory control sets the engine-out NO <sub>x</sub> target for the engine module, accounting for ATS state. A control-oriented engine model is used.	The strategy was tested on a GT-POWER engine model, and the results show that it is effective in fulfilling the emission legislation limits.

The main novelty proposed in this paper consists of the use of a physics-based real-time combustion model, which was validated on the road in [15] and is capable of adjusting the injected fuel quantity and injection timing of the main pulse in order to achieve desired targets of BMEP and engine-out NO<sub>x</sub> levels to explore two different approaches for the calibration and control of tailpipe NO<sub>x</sub> emissions in a 3.0 L heavy-duty diesel engine. These approaches are highly computationally efficient and therefore have the potential of being implemented in an engine control unit.

The first approach consists of a model-based offline calibration strategy, which minimizes an objective function that takes into account fuel consumption and AdBlue injection and identifies specific targets of engine-out NO<sub>x</sub> emissions for the combustion controller on the basis of steady-state simulations.

The second approach is a dynamic online strategy, which is based on a direct model-based controller of tailpipe nitrogen oxide emission. The controller exploits the instantaneous value of the SCR efficiency to define engine-out NO<sub>x</sub> emission targets for the combustion controller in real-time.

Both strategies were tested through Model-in-the-Loop (MiL) on a validated model of a 3.0 L heavy-duty diesel engine, which was realized in GT-SUITE environment. Steady-state and transient tests were considered.

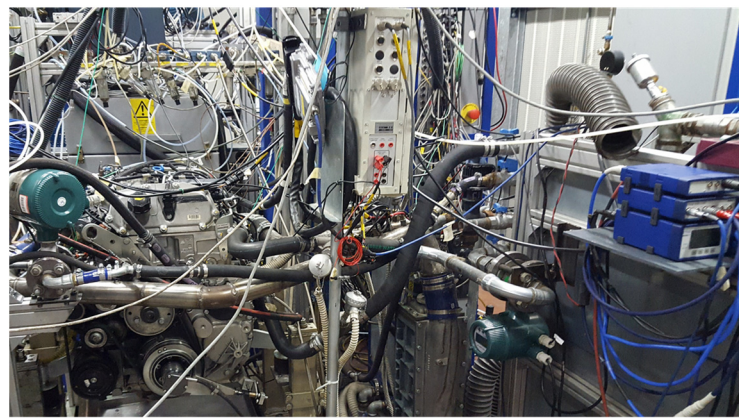
## 2. Experimental Setup and Engine Conditions

A 3.0 L Euro VI diesel engine was considered in this study. The main engine specifications are reported in Table 2.

The experimental tests, which were used for the tuning of the GT-SUITE engine model and the models used in the combustion controller, were carried out on the dynamic test rig at ICEAL-PT (Internal Combustion Engines Advanced Laboratory at the Politecnico di Torino). A picture of the engine is reported in Figure 1.

**Table 2.** Main technical specifications of the engine.

Engine Specifications	
Engine type	Euro VI diesel engine
Number of cylinders	4
Displacement	2998 cm <sup>3</sup>
Bore × stroke	95.8 mm × 104 mm
Rod length	160 mm
Compression ratio	17.5
Valves per cylinder	4
EGR	Short-route type, with cooler
Turbocharger	VGT type
Exhaust flap valve	Located at the turbine outlet
Fuel injection system	High-pressure Common Rail

**Figure 1.** Picture of the 3.0 L Euro VI diesel engine.

The details on the engine instrumentation can be found in [16] and have not been reported here for the sake of brevity.

The test bench is equipped with an ‘ELIN AVL APA 100’ AC dynamometer and an ‘AVL KMA 4000’ fuel meter, that features a relative accuracy of 0.1% in the 0.28–110 kg/h range. An ‘AVL AMAi60’ was used to measure the concentrations of HC, CH<sub>4</sub>, NO<sub>x</sub>/NO, CO, CO<sub>2</sub>, and O<sub>2</sub> both at the intake and exhaust sides, and another train was dedicated to the measurement of the CO<sub>2</sub> concentration in order to derive the EGR rate. Finally, an ‘AVL 415S’ smoke meter was used to measure soot in steady-state conditions, whereas an ‘AVL 439’ opacimeter was available for transient measurements. The PUMA OPEN 1.3.2 automation system was used to control all the devices.

#### Experimental Activity

The experimental test results acquired at the test bench were previously used for the calibration of the GT-SUITE engine model [31] and the real-time models used for the combustion controller [16,38] for the same engine. These tests were already reported in [16,38] and include (Figure 2):

- A complete engine steady-state map including 123 points.
- EGR-sweep tests at fixed key points, in which the EGR rate was varied in the 0–50% range. A total of 162 tests was acquired.
- sweep tests of main injection timing (SOI<sub>main</sub>) and injection pressure (p<sub>f</sub>) at fixed key-points, in which the SOI<sub>main</sub> and p<sub>f</sub> were varied of ±6 deg and ±20% around the baseline values, respectively. A total number of 125 points was acquired.

Table 3 reports the fuel specifications.



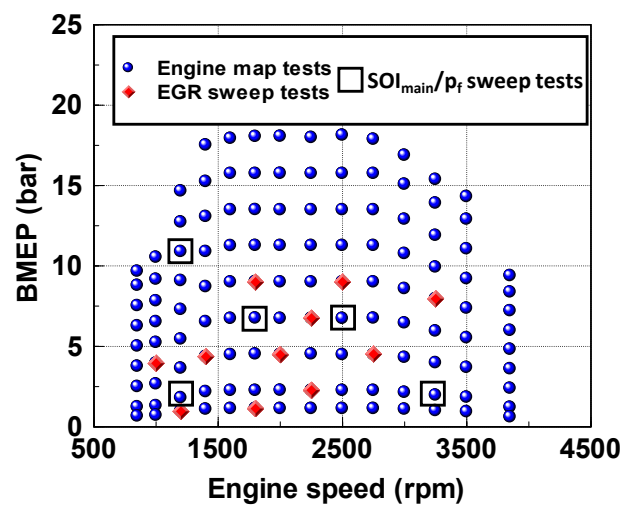


Figure 2. Summary of the experimental tests.

Table 3. Main properties of the diesel EN590 fuel.

Property	Units	Diesel EN 590
Cetane number		53.1
Flash Point	°C	70
Density at 15 °C	kg/m <sup>3</sup>	844
Viscosity at 40 °C	mm <sup>2</sup> /s	2.86
Distillation 50% vol	°C	273
Distillation 95% vol	°C	351
Final boiling point	°C	363
Evaporated at 250 °C	% vol	36
FAME	% vol	6.9
Sulphur	ppm	8
PAHs	% mass	3.7
Lower heating value	MJ/kg	43.4

### 3. Model Description

The engine model is described in Section 3.1, while Section 3.2 shortly describes the combustion controller integrated in the engine model. Section 3.3 reports the developed offline and online calibration strategies.

#### 3.1. Engine Model

A fast-running engine model, developed in GT-SUITE environment, was used in this paper for the assessment of the proposed calibration and control strategies of tailpipe NO<sub>x</sub> emissions. The model scheme is reported in Figure 3.

The ATS scheme includes the DOC, DPF, and SCR submodels, as well as the AdBlue injection controller, which calculates the AdBlue mass flow rate to be injected at each time instant as a function of the NO<sub>x</sub> concentration detected upstream of the SCR system. The AdBlue injection controller requires setting the parameter  $\alpha = \frac{n_{NH_3}}{n_{NO_x}}$ , in which  $n_{NH_3}$  is the molar flow rate of ammonia injected upstream of the SCR system and  $n_{NO_x}$  is the molar flow rate of NO<sub>x</sub> upstream of the SCR system. In this study,  $\alpha$  has been fixed to 1 in order to allow the highly efficient operation of the SCR device without a risk of ammonia slip.

It should be noted that the efficiency of the SCR device mainly depends on three physical quantities: AdBlue flow rate, average SCR temperature, and the NO/NO<sub>2</sub> ratio in the exhaust gases upstream of the SCR system.

The AdBlue flow rate depends linearly on the NO<sub>x</sub> concentration upstream from the SCR, since the  $\alpha$  parameter has been set to 1 in this study.

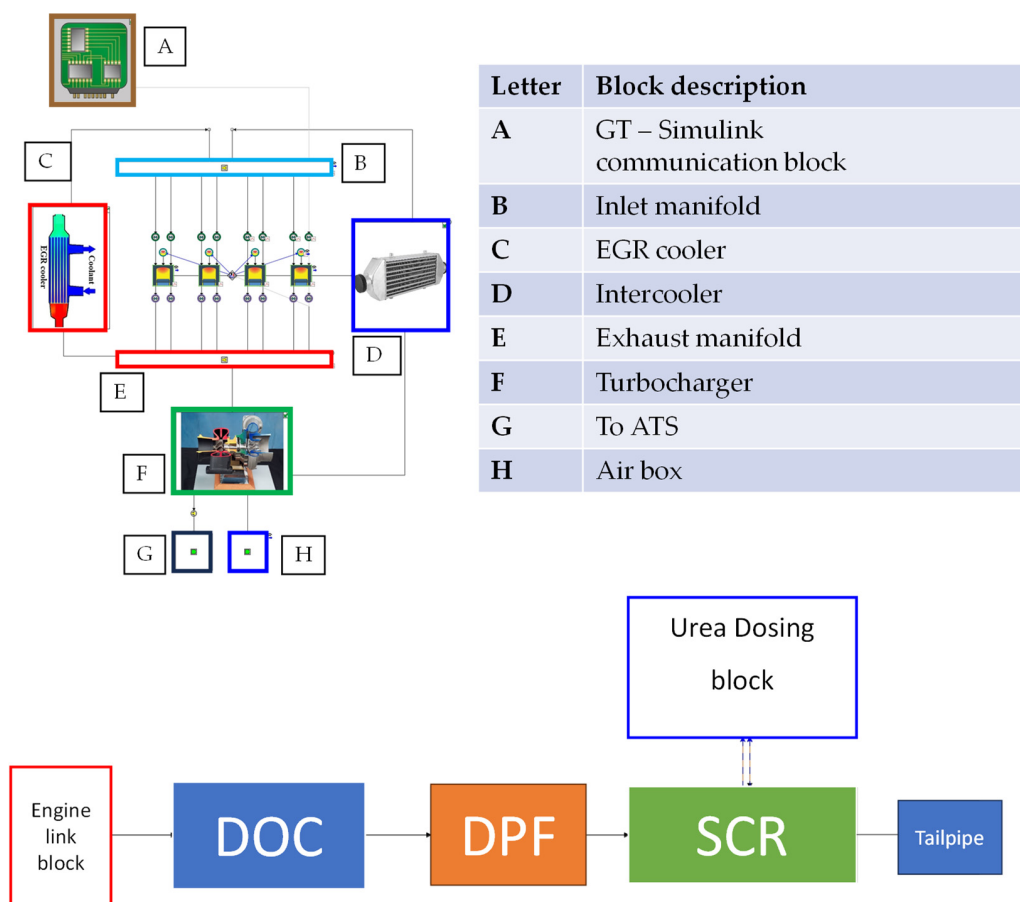


**Figure 3.** Scheme of the engine model realized in GT-SUITE.

The average SCR temperature depends on the exhaust gases temperature. The SCR system has shown to have acceptable efficiencies in the 230–450 °C range, so the AdBlue flow rate is cut off by the controller in the case that the upstream SCR system temperature is lower than 200 °C.

The NO/NO<sub>2</sub> ratio has a great impact on the SCR efficiency [39] and is controlled via the DOC, whose model has been fine tuned to raise the downstream NO<sub>2</sub> concentrations in the exhaust gases to the highest possible value so as to enhance the SCR efficiency.

Table 4 reports a summary of the specifications of the DOC, DPF, and SCR implemented in the model.

**Table 4.** Main specifications of DOC, DPF, and SCR.

Property	DOC	DPF	SCR
Frontal diameter (mm)	150	150	130
Length (mm)	150	600	500
Cell density 1/inch <sup>2</sup>	400	150	400
Substrate wall thickness (mil thou)	4	17	6.5
Washcoat thickness (µm)	40	-	-

The fast-running engine model was previously calibrated using the experimental tests acquired at the test bench for the considered engine [31], except for the ATS system, which was not installed at the test rig. The ATS was instead modeled and tuned on the basis of the guidelines and data which were reported in the GT-SUITE manuals.

The validation results of the fast-running engine model, as well as the performance results of the SCR device, are shown in Appendix A.

### 3.2. Model-Based Combustion Controller

The model-based combustion controller was already presented in previous studies, when it was applied to the same engine [16] and also to a 11.0 L diesel engine within the IMPERIUM H2020 European Collaborative Research Project [15], during which it was implemented on the road. However, a description of the controller is also briefly provided in the present paper for the sake of clarity. The conceptual scheme of the control algorithm is reported in Figure 4.

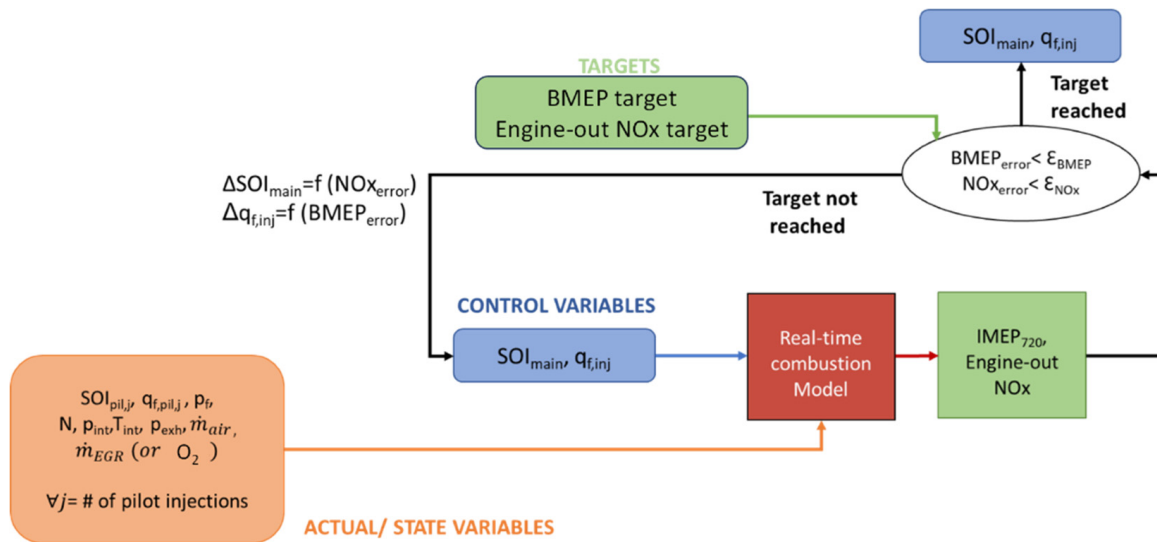


Figure 4. Conceptual scheme of the controller.

The controller acts on two control variables, i.e., the injected quantity ' $q_{f,inj}$ ' and the injection timing of the main pulse ' $SOI_{main}$ ', in order to match the desired targets of BMEP and engine-out NOx concentration. An iterative procedure is used, along which the values of the control variables are adjusted on the basis of the error between the simulated values of BMEP and NOx and the related targets. Convergence is achieved within a single engine firing (i.e.,  $720^\circ$  CA divided by the number of the cylinders) and occurs when the BMEP and NOx errors are below two user-defined thresholds, which are indicated as  $\epsilon_{BMEP}$  and  $\epsilon_{NOx}$ , respectively. The selection of the injection timing of the main pulse as a control variable allows to potentially achieve a cycle-by-cycle NOx control, as reported in [15,16]. It can also be seen in Figure 4 that the controller requires several state variables as inputs. Additional details are reported in [16].

In this study, the engine-out NOx target ' $NOx_{EO\_TGT}$ ' was translated into an engine-out NOx multiplier, as follows:

$$NOx_{EO\_Mult} = \frac{NOx_{EO\_TGT}}{NOx_{EO\_TGT\_base}} \quad (1)$$

where ' $NOx_{EO\_TGT\_base}$ ' is the baseline engine-out NOx target, which is defined by a lookup table as function of engine speed and load and was derived by the emitted engine-out NOx levels when the engine operates under nominal conditions.

The combustion controller is switched off when the required BMEP is lower than the threshold of 0.5 bar since the model accuracy deteriorates significantly at very low load conditions. When the combustion controller is disabled, the engine operates with nominal parameters.

The detailed description of the combustion model can be found in [16] and its scheme is described in Figure 5.

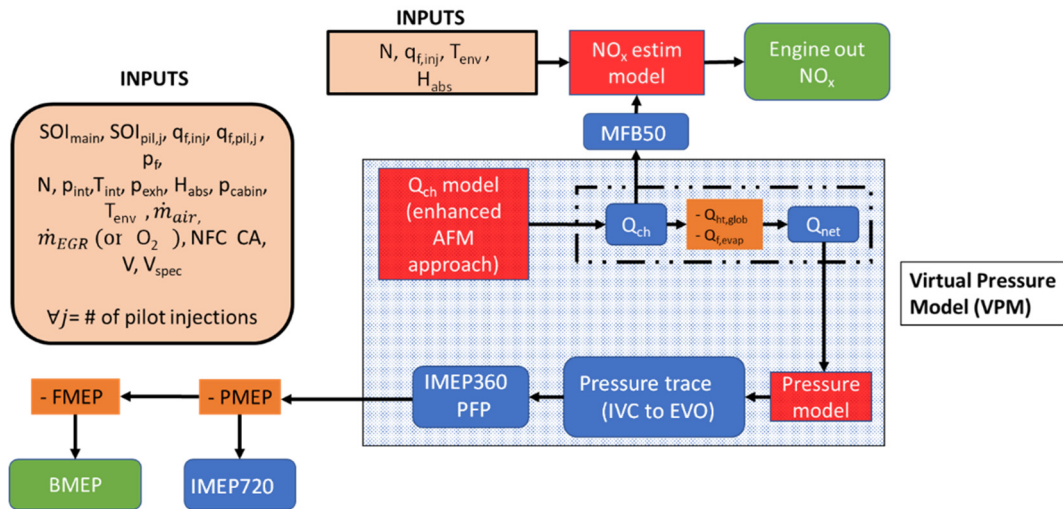


Figure 5. Scheme of the combustion model.

It can be seen in the figure that the model starts from the simulation of the chemical energy release ( $Q_{ch}$ ) by adopting the accumulated fuel mass (AFM) approach, and evaluates the net energy release ( $Q_{net}$ ) by accounting for fuel evaporation and heat transfer. The in-cylinder pressure is then simulated through a single-zone thermodynamic model and is used to derive the gross indicated mean effective pressure 'IMEP360'. Finally, pumping losses (PMEP) and friction losses (FMEP) are obtained from a semi-empirical correlation and from the Chen–Flynn method, respectively, and this allows for the evaluation of BMEP starting from IMEP360. A semi-empirical model [38] is finally adopted to estimate the engine-out NOx concentration.

The detailed description of each sub-model is not here reported for the sake of brevity, but it is reported in [16] for the same engine. Only some details related to the NOx model are reported hereafter. Full details about the development and calibration of the NOx model for the same engine are reported in [38].

The modeling approach is based on the sum of two contributions: the nominal NOx value ' $NOx_N$ ' which is emitted by the engine when it operates at nominal conditions (in terms of engine calibration parameters) and a NOx deviation ' $\delta NOx$ ', which occurs when MFB50 or the intake  $O_2$  concentration deviate with respect to the nominal values  $MFB50_N$  and  $O_{2N}$ . The nominal values of NOx emissions, MFB50, and  $O_2$  have been tabulated as a function of engine speed ' $N$ ' and total injected quantity ' $q_{f,inj}$ ', and these tables are based on the measurements performed at steady-state conditions. More in detail, the NOx have been modeled as follows:

$$NOx = NOx_N(N, q_{f,inj}) + \delta NOx(\delta MFB50, \delta O_2, N, q_{f,inj}) \quad (2)$$

$$\delta NOx = a_1 \cdot \left[ -abs(\delta MFB50)^{a_2} \cdot sign(\delta MFB50) + a_3 \delta O_2 \right] \cdot q_{f,inj}^{a_4} \cdot N^{a_5} \quad (3)$$

$$\delta MFB50 = MFB50 - MFB50_N(N, q_{f,inj}); \quad \delta O_2 = O_2 - O_{2N}(N, q_{f,inj}) \quad (4)$$

Equations (2)–(4) were derived assuming that the main variation of NOx emissions with respect to the engine map values can be explained by a combustion phasing variation and charge oxygen variation. The injected fuel mass and the engine speed are used as multiplicative terms since it was observed experimentally that the range of the NOx deviations increases with engine load and is also affected by engine speed.

Equations (2)–(4) were also derived under the assumption that that a positive variation of MFB50 (i.e., a more delayed combustion) leads to the negative variation of NOx, and that a positive variation of  $O_2$  leads to a positive variation of NOx. These assumptions can

be considered reasonable for most of the operating conditions which occur in conventional diesel combustion. The previous equations are valid for a given set of ambient temperature and humidity  $T_{env}$ ,  $H_{abs}$ . If the model is applied to predict NOx emissions when the ambient conditions are varied (e.g., to ' $T_{env}$ ' and ' $H_{abs}$ '), the NOx are corrected according to the recommended practice proposed in [40].

### 3.3. Developed Strategies for Tailpipe NOx Control

Two distinct strategies have been developed in this paper for the calibration and control of tailpipe NOx emissions. The first one, which is described in Section 3.3.1, is an offline calibration approach which defines optimal targets of engine-out NOx through a static map. The second one, which is described in Section 3.3.2, involves an online calibration, which is based on a model-based controller that has the aim of achieving a specified tailpipe NOx target while keeping the desired torque by acting on the  $SOI_{main}$  and  $q_{f,inj}$  control variables. It is noteworthy that both strategies rely on the real-time model-based combustion controller which was described in the previous section, for which they set a proper engine-out NOx target through the ' $NOx\_EO\_Mult$ ' control variable. In general, the values of this variable were constrained in the [0.5–1.5] range. This restriction was implemented in order to prevent engine operation under infeasible conditions arising from excessively advanced or retarded  $SOI_{main}$  values. Excessively advanced  $SOI_{main}$  values can lead to uncontrolled combustion and excessive peak firing pressure, while retarded  $SOI_{main}$  values can result in incomplete combustion and high exhaust temperatures. This limitation ensures optimal engine operation and safeguards against potential damages.

#### 3.3.1. Offline Calibration Strategy

The objective of this strategy is to determine the optimal engine-out NOx emission targets by balancing fuel consumption and AdBlue injection across a simulated engine map. This is realized by minimizing an objective function ' $F$ ', which is defined as follows:

$$F = \beta \cdot \frac{BSFC}{BSFC_{NOM}} + (1 - \beta) \frac{\dot{m}_{ADBLUE}}{\dot{m}_{ADBLUE, NOM}}; \beta \in [0; 1] \quad (5)$$

where BSFC indicates the brake specific fuel consumption and  $\dot{m}_{ADBLUE}$  the instantaneous mass consumption of AdBlue, whereas  $BSFC_{NOM}$  and  $\dot{m}_{ADBLUE, NOM}$  designate the BSFC and  $\dot{m}_{ADBLUE}$  from the baseline engine simulation, which was carried out by setting the NOx multiplier equal to 1. The choice to include fuel consumption and AdBlue consumption in the definition of the objective function is justified since the two quantities are closely correlated with the variable operating costs, which are a key aspect for heavy-duty applications. In Equation (5), ' $\beta$ ' is an adjustable weight factor whose value can vary in the [0, 1] range and is decided by the user to identify calibration strategies which are more or less oriented to BSFC minimization or AdBlue consumption minimization.

It should be noted that BSFC and  $\dot{m}_{ADBLUE}$  are functions of the engine-out NOx multiplier ' $NOx\_EO\_Mult$ ', which is used to define the engine-out NOx target for the combustion controller according to Equation (1). This can be justified considering that the combustion controller modulates ' $SOI_{main}$ ' on the basis of the engine-out NOx target (as well as ' $q_{f,inj}$ ' to achieve the desired BMEP), and the two control variables directly affect the BSFC value. In addition, the engine-out NOx level also affects the AdBlue injection rate, which is decided by the SCR controller (see Figure 3), since higher engine-out NOx concentrations correspond to a higher number of  $NH_3$  moles which are requested for NOx reduction. Therefore, in the end, the whole objective function depends on the engine-out NOx multiplier ' $NOx\_EO\_Mult$ '.

This can be seen in Figure 6, which shows the dependence of the BSFC and  $\dot{m}_{ADBLUE}$  (Figure 6a) and of the objective function ' $F$ ' (Figure 6b) on the engine-out NOx multiplier, at  $N = 3000$  rpm and  $BMEP = 9$  bar.

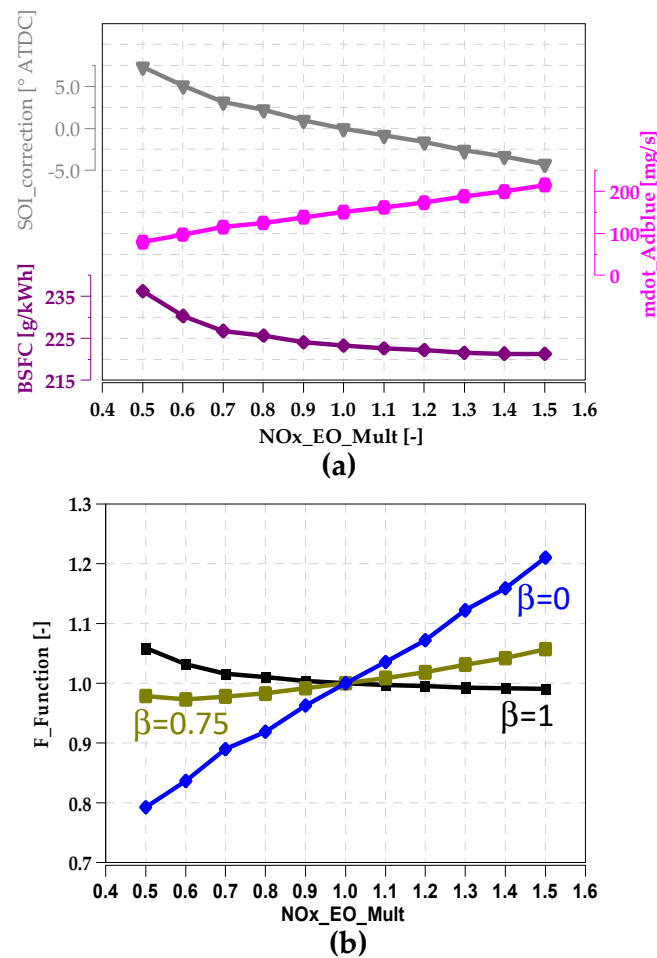


**Figure 6.** Trends of the BSFC, AdBlue (a), and the objective function 'F' (b) as a function of the engine-out NOx multiplier 'NOx\_EO\_Mult' at N = 3000 rpm and BMEP = 9 bar.

Higher values of 'NOx\_EO\_Mult' are associated with a request for higher levels of engine-out NOx, and this leads to the selection of more anticipated values of 'SOI<sub>main</sub>' by the combustion controller, which generally determine the lower values of BSFC and higher levels of AdBlue consumption (as can be seen in the example of Figure 6a), and vice versa. Instead, the trend of 'F' as a function of 'NOx\_EO\_Mult' depends on the choice of ' $\beta$ ' to a great extent, as can be seen in Figure 6b.

In order to explore the influence of ' $\beta$ ' on the values of the weight function, several simulations were carried out all over the engine map by changing, for each engine point, the engine-out NOx target (i.e., by acting on the engine-out NOx multiplier 'NOx\_EO\_Mult'), and estimating the value of the objective function 'F'. The tests were repeated for different values of ' $\beta$ '.

Some results are shown in Figure 7, which reports the trend of the objective function 'F', as a function of 'NOx\_EO\_Mult', at four different engine operating points, considering five different values of ' $\beta$ '.

The results in Figure 7 show that the shape of the trend of the objective function depends on  $\beta$  to a great extent. It should be noted that the choice of  $\beta = 1$  corresponds to a full BSFC-oriented optimization, while the choice of  $\beta = 0$  corresponds to a full AdBlue-oriented optimization. All the results were obtained with a fixed value of  $\alpha = 1$  in the SCR controller.

It can be noted in the figure that, for values of  $\beta$  which are lower than 0.95, the minimization of F always leads to the selection of the minimum NOx multiplier value (i.e., 0.5), which corresponds to the minimum allowed value of the engine-out NOx target. As a

matter of fact, an optimization that is oriented to AdBlue minimization requires low values of engine-out NO<sub>x</sub> emissions, since the AdBlue injected mass is directly correlated to the number of NO<sub>x</sub> moles that enter the SCR device (for a fixed value of  $\alpha = 1$ ).

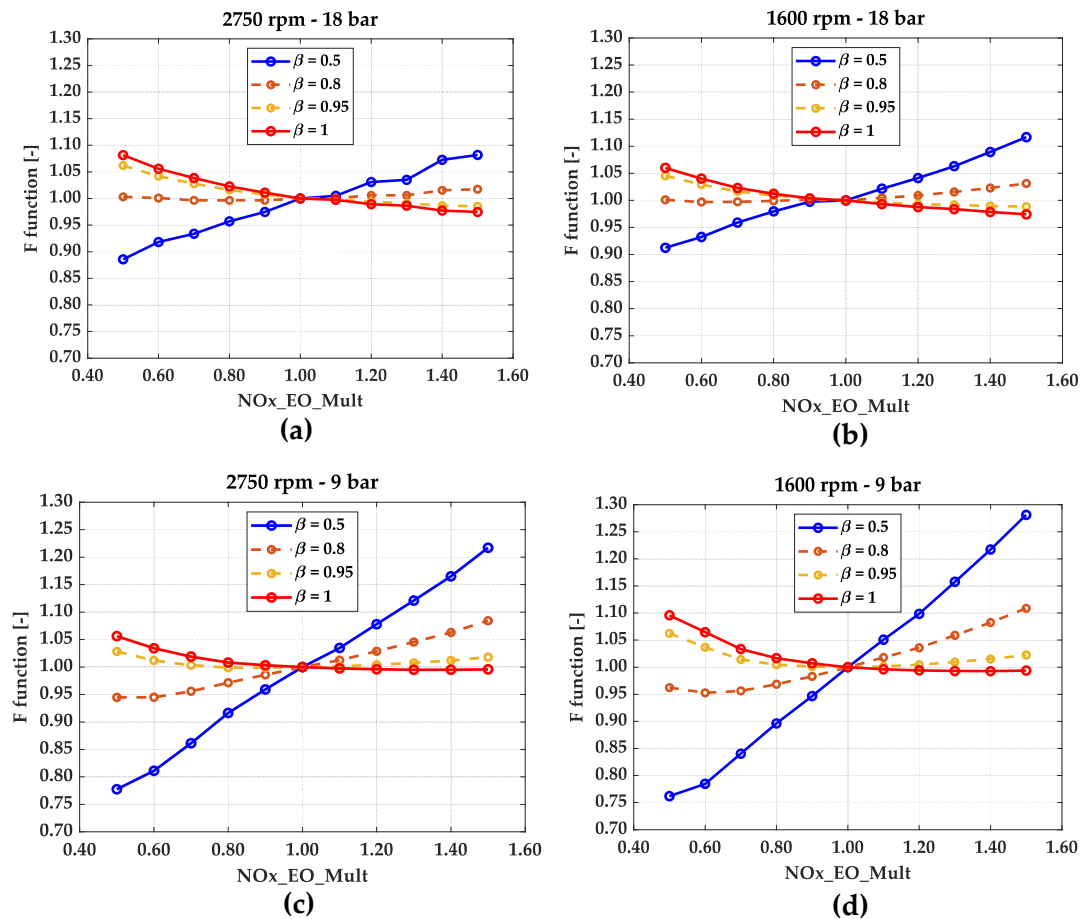


**Figure 7.** Trends of the objective function ‘F’ as a function of the engine-out NO<sub>x</sub> multiplier ‘NO<sub>x</sub>, EO, Mult’ at four different engine operating points, considering different values of ‘ $\beta$ ’. The numbers above each figure define the operating point as N (rpm)  $\times$  BMEP (bar).

The minimum value of the objective function was selected for each simulated engine operating point and for several values of  $\beta$ , and the corresponding values of the NO<sub>x</sub> multiplier were stored in a lookup table as a function of engine speed and BMEP. Therefore, several lookup tables were defined, corresponding to different values of  $\beta$ , ranging from  $\beta = 1$  (full BSFC oriented optimization) to  $\beta = 0$  (full AdBlue-oriented optimization). These lookup tables were implemented in the engine model and tested under steady-state and transient operation over a WHTC.

As an example, Figure 8 reports contour plots of the differences between the values of NO<sub>x</sub> multiplier obtained from the objective function minimization over the whole engine map (with  $\beta = 1$  and  $\beta = 0.95$ ) and the baseline value, equal to 1.

It can be seen that the optimization leads to generally higher values of the NO<sub>x</sub> multiplier at higher loads (corresponding to a request of higher engine-out NO<sub>x</sub> levels) and to lower values at lower loads. The engine-out NO<sub>x</sub> request decreases in the case of  $\beta = 0.95$  due to the contribution of the AdBlue consumption term in the weight function.

Figures 9 and 10 report the contour plots of the variations in the values of BSFC and AdBlue mass flow rate with respect to the baseline case (Figure 9) as well as the engine-out/tailpipe NO<sub>x</sub> concentrations (Figure 10), obtained by applying the lookup tables of the NO<sub>x</sub> multiplier which were derived from the objective function minimization (with  $\beta = 1$  and  $\beta = 0.95$ ).

### ΔNOx multiplier

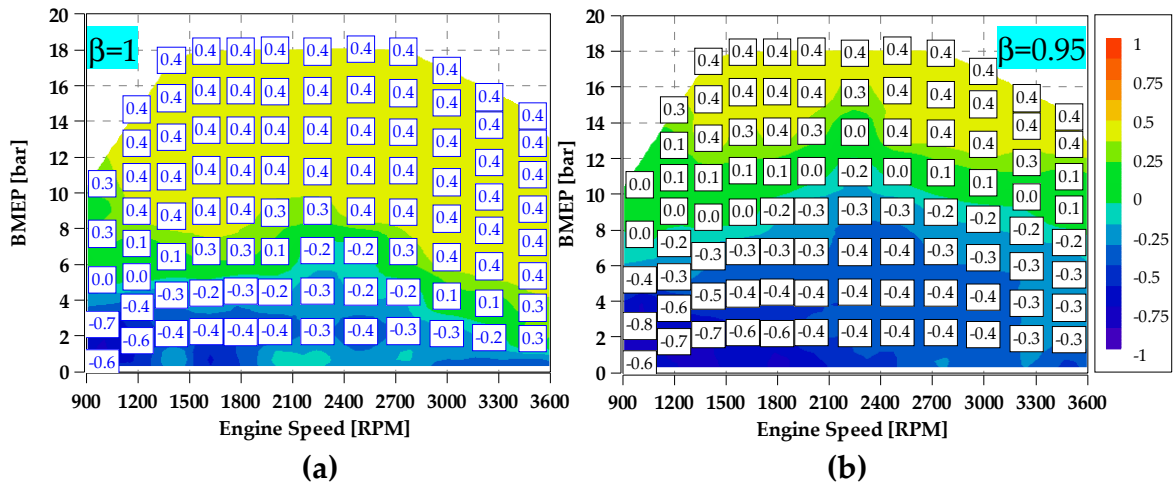
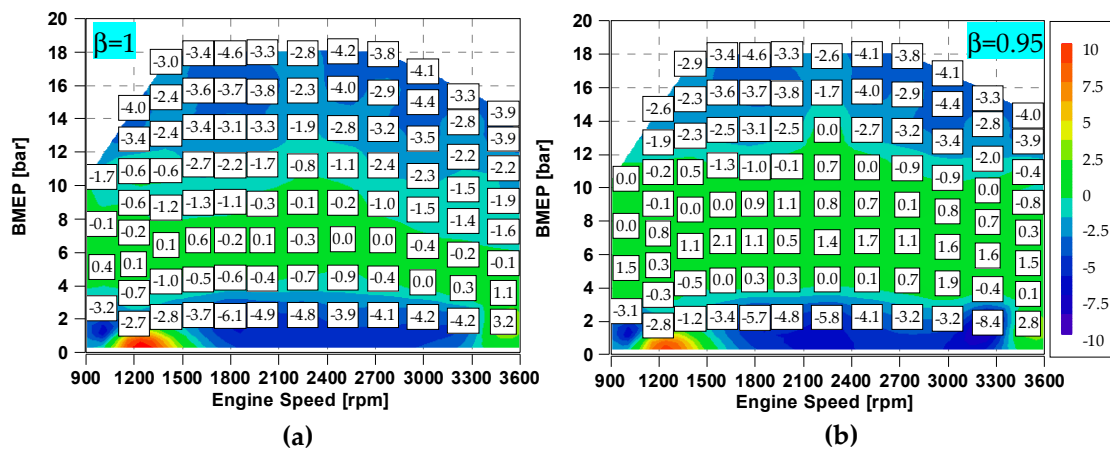


Figure 8. Contour plots of the differences between the values of NOx multiplier obtained with the objective function minimization over the whole engine map (with  $\beta = 1$  (a) and  $\beta = 0.95$  (b)) and the baseline value equal to 1.

### ΔBSFC (g/kWh)



### ΔAdBlue (g/kWh)

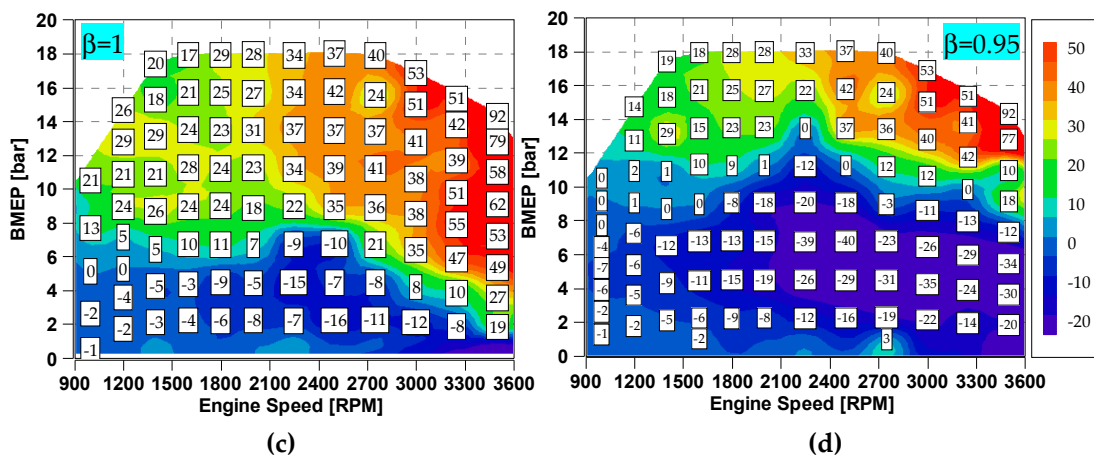
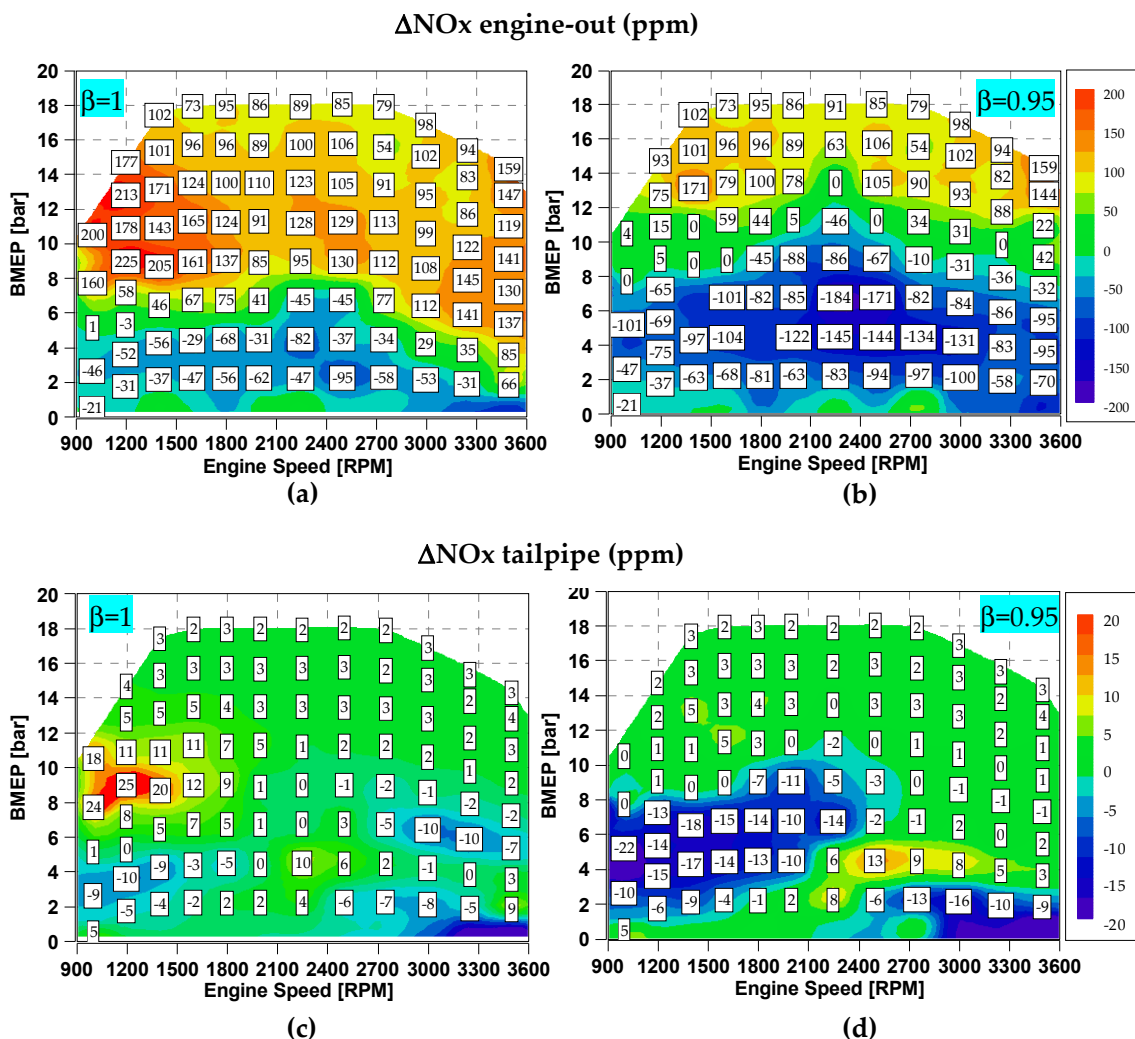


Figure 9. Contour plots of the variations with respect to the baseline case over the whole engine map of the values of BSFC (a,b) and AdBlue mass flow rate (c,d), obtained by applying the lookup tables of the NOx multiplier obtained with the objective function minimization (with  $\beta = 1$  and  $\beta = 0.95$ ).





**Figure 10.** Contour plots of the variations with respect to the baseline case over the whole engine map of the values of engine-out NOx emissions (a,b) and tailpipe NOx emissions (c,d), obtained by applying the lookup tables of the NOx multiplier obtained with the objective function minimization (with  $\beta = 1$  and  $\beta = 0.95$ ).

It can be seen in the figures how the adoption of a full BSFC-oriented optimization ( $\beta = 1$ ) leads to generally higher engine-out NOx emissions with respect to the baseline case, especially at medium-high loads (Figure 10a), which is mainly due to the selection of more anticipated values of  $SOI_{main}$  by the combustion optimizer. The most significant improvements in terms of BSFC<sub>main</sub> at higher loads (Figure 9a), where it can be observed that the reduction in BSFC does not correspond to a substantial variation in tailpipe NOx emissions (Figure 10c). In other words, this strategy allows full saturation of the SCR system reduction capabilities.

When considering a more balanced objective function ( $\beta = 0.95$ ), it can be seen that the AdBlue mass flow rate generally decreases with respect to the baseline value (Figure 9d), and the NOx multiplier and NOx engine-out values are also lower (Figure 10b,d), while higher BSFC values occur (Figure 9b).

By summarizing, the proposed calibration strategy allows for the identification of several lookup tables of the NOx multiplier (and, therefore, of the engine-out NOx target) for different values of the weight factor  $\beta$ .

Higher  $\beta$  values will lead to lower BSFC values, to higher levels of engine-out NOx emissions (and, therefore, of AdBlue consumption), as well as to higher tailpipe NOx emissions, and vice versa.

The choice of the weight factor  $\beta$  is made by the user, depending on the BSFC-tailpipe NOx trade-off that is desired.

### 3.3.2. Online Calibration Strategy

The second method which is investigated in this paper consists of an online calibration strategy, which relies on a tailpipe NOx controller. This strategy is based on the estimation of the actual value of the SCR efficiency, which is calculated as follows:

$$SCR_{eff, meas} = \frac{NOx_{EO\_meas} - NOx_{TP\_meas}}{NOx_{EO\_meas}} \quad (6)$$

where ' $NOx_{EO\_meas}$ ' and ' $NOx_{TP\_meas}$ ' indicate the actual values of the engine-out and tailpipe NOx concentrations, respectively. The SCR efficiency is estimated at each time instant from the acquisition of the NOx concentration upstream and downstream of the SCR system.

A target of tailpipe NOx emission ' $NOx_{TP\_TGT}$ ' is then defined.

On the basis of the measured SCR efficiency, the tailpipe NOx target is translated into an engine-out NOx target by inverting Equation (6) and replacing ' $NOx_{EO\_meas}$ ' with ' $NOx_{EO\_TGT}$ ' and ' $NOx_{TP\_meas}$ ' with ' $NOx_{TP\_TGT}$ ', as follows:

$$NOx_{EO\_TGT} = \frac{NOx_{TP\_TGT}}{1 - SCR_{eff, meas}} \quad (7)$$

The engine-out NOx target is then used to evaluate the engine-out NOx multiplier, which is given to the combustion controller as input (see Equation (1)).

In this study, the targets of tailpipe NOx emissions were derived from the simulation of the baseline engine map (with  $NOx_{EO\_Mult} = 1$ ), and stored in a lookup table as a function of engine speed and BMEP, which was then integrated in the controller.

By analyzing Equation (7), it can be noted that if the values of ' $NOx_{TP\_TGT}$ ' or ' $SCR_{eff, meas}$ ' are too low, ' $NOx_{EO\_TGT}$ ' tends to assume unfeasibly low values, which lead the combustion controller to heavily retard the injection timing and, therefore, the combustion phasing. Conversely, if the values of ' $SCR_{eff, meas}$ ' are high and become close to 1, ' $NOx_{EO\_TGT}$ ' tends to assume excessively high values, so that the combustion controller tends to anticipate the injection timing to a great extent.

Finally, it should be noted that the current version of the online calibration strategy does not take into account a dedicated algorithm for BSFC or AdBlue minimization over a specific driving mission; therefore, the actual fuel and AdBlue consumption are functions of the selected tailpipe NOx targets. Future work will explore the possibility of accounting for limits in terms of BSFC penalization or AdBlue consumption for the definition of optimal tailpipe NOx targets.

Figure 11 reports the scheme of the online NOx calibration strategy: the baseline tailpipe NOx emission targets are stored in a map. The value of the SCR efficiency ' $SCR_{eff\_meas}$ ' is calculated at each time instant and used to derive the engine-out NOx target ' $NOx_{EO\_TGT}$ ', which in turn is used to calculate the engine-out NOx multiplier ' $NOx_{EO\_Mult}$ '. Finally, this value is given to the combustion controller for  $SOI_{main}$  and  $q_{f, inj}$  regulation.

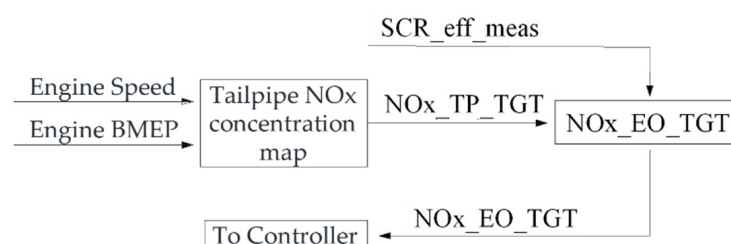


**Figure 11.** Scheme of the online NOx calibration strategy.

#### 4. Results and Discussion

In this section, the main results of the performance of the two developed strategies are shown and compared over a hot WHTC and mild load ramps.

##### 4.1. Simulation of a WHTC

First, the offline calibration strategy has been tested over the WHTC by adopting different values of  $\beta$  ranging from 0 to 1, while the online calibration strategy has been tested by setting the nominal tailpipe NOx target (obtained from the baseline engine operation), and different target offsets, in a range between  $-50\%$  and  $+500\%$ . All the results have been compared with the baseline strategy, in which the NOx multiplier was set equal to 1 all over the engine map. Tables 5 and 6 present the results for the offline and online calibration strategies, respectively, over the WHTC, in terms of BSFC, engine-out and tailpipe bsNOx and bsAdBlue consumption. The tables also report the mean value of the engine-out NOx multiplier that was selected by the two strategies over the WHTC.

**Table 5.** Results of the offline strategy over the hot WHTC for different values of  $\beta$  and comparison with the baseline calibration ( $NOx\_EO\_Mult = 1$ ).

353BImposed $\beta$	354BMean 355BNOx_EO_Mult	356BBSFC	357BbsNOx Engine-Out	358BbsNOx Tailpipe	359Bbs AdBlue
360B-	361B-	362Bg/kWh	363Bg/kWh	364Bg/kWh	365Bg/kWh
366B1	367B0.82	368B232.3	369B4.26	370B0.64	371B8.1
372B0.95	373B0.7	374B233.3	375B3.48	376B0.55	377B6.7
378B0.9	379B0.63	380B235.8	381B2.96	382B0.47	383B5.7
384B0.8	385B0.54	386B242.3	387B2.27	388B0.36	389B4.6
390B0.6	391B0.52	392B245.8	393B2.06	394B0.33	395B4.6
396B0	397B0.5	398B245.8	399B2.06	400B0.33	401B4.6
n.a.	1 (baseline)	404B233.9	405B3.93	406B0.62	407B8

**Table 6.** Results of the online calibration strategy over the hot WHTC by setting nominal NOx target (obtained from baseline engine operation) and different target offsets (in a range between  $-50\%$  and  $+500\%$ ) and comparison with the baseline calibration ( $NOx\_EO\_Mult = 1$ ).

409BTailpipe NOx Target Offset	410BMean NOx_EO_ Mult	411BBSFC	412BbsNOx Engine-Out	413BbsNOx Tailpipe	414Bbs 415BAdBlue	416B $\Delta$ NOx Engine-Out 417B (Actual)	418B $\Delta$ NOx Tailpipe (Actual)
419B	420B	421Bg/kWh	422Bg/kWh	423Bg/kWh	424Bg/kWh	425B%	426B%
427B500%	428B1.3	429B234.7	430B5.4	431B0.65	432B12.1	433B29%	434B41%
435B325%	436B1.3	437B235.4	438B5.2	439B0.6	440B11.6	441B25%	442B31%
443B300%	444B1.2	445B235.5	446B5.2	447B0.59	448B11.4	449B25%	450B29%
451B200%	452B1.2	453B236.3	454B5	455B0.55	456B9.7	457B19%	458B20%
459B175%	460B1.1	461B236.6	462B4.8	463B0.54	464B9.5	465B17%	466B17%
467B50%	468B1.1	469B237.1	470B4.7	471B0.52	472B9.2	473B13%	474B14%
475B0%	476B1.0	477B238.6	478B4.1	479B0.46	480B8.2	481B0%	482B0%
483B $-50\%$	484B0.8	485B241	486B3.4	487B0.38	488B6.7	489B $-18\%$	490B $-16\%$
491B (Baseline)	492B1.0	493B233.9	494B3.93	495B0.62	496B8	497B/	498B/

The last two columns of Table 6 indicate the actual integral variation of engine-out and tailpipe NOx with respect to the case in which the nominal target of the controller is set (i.e., target offset  $0\%$ ) over the WHTC.

First, the two strategies have been compared in terms of BSFC-tailpipe bsNOx trade-offs, which have been reported in Figure 12.

The BSFC-tailpipe NOx trade-off obtained with the offline calibration strategy is overall better, even though the curve related to the use of the online strategy intersects the previous curve at a tailpipe bsNOx level around  $0.43$  g/kWh, and this may lead to advantages for lower bsNOx values.

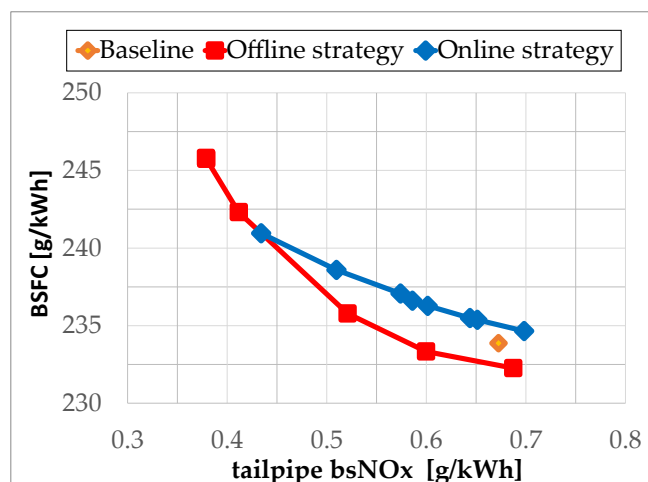


**Figure 12.** Comparison of the BSFC- tailpipe NO<sub>x</sub> trade-offs obtained with the offline calibration strategy (red line) and with the online calibration strategy (blue line) for the simulations of the WHTC. The results of the baseline calibration strategy are also reported with an orange diamond.

The offline strategy allows for the flexibility to select different optimizations in terms of BSFC and AdBlue consumption (by changing the value of  $\beta$ ), which can be more BSFC-oriented or AdBlue (and tailpipe NO<sub>x</sub>)-oriented. A preliminary analysis of the total cost of ownership (TCO) showed that, minimizing this parameter corresponds to minimizing the fuel consumption, as the price per Liter of AdBlue is lower than that of fuel, while the mass fuel consumption is much higher. The choice  $\beta = 1$  leads to the minimization of the TCO, but other strategies could be considered also customer-oriented, such as, increasing the mileage of the vehicle between two consecutive refills of AdBlue.

Concerning the online calibration strategy, it can be seen in Figure 12 that, in this case, the BSFC-tailpipe NO<sub>x</sub> trade-off tends to deteriorate slightly with respect to the baseline point, which is below the trade-off curve. The reason for this slight deterioration could be related to the fact that the combustion controller receives engine-out NO<sub>x</sub> targets which are frequently on the boundary (i.e., very high or very low), and this could lead to non-optimal engine conditions in terms of thermal efficiency. However, an advantage of the proposed approach is the possibility of directly targeting a desired value of tailpipe NO<sub>x</sub> emissions, and the combustion controller can dynamically adapt the injection parameters in real-time, in order to achieve the targets. Moreover, as can be seen in Table 6, a monotonic trend exists between the actual integral variation of tailpipe NO<sub>x</sub> ( $\Delta\text{NO}_x$  Tailpipe (actual)', last column) and the tailpipe NO<sub>x</sub> target offset which is requested ('Tailpipe NO<sub>x</sub> target offset', first column). This trend can be used to decide the NO<sub>x</sub> target offset to be set in the controller in order to achieve a desired actual integral variation of tailpipe NO<sub>x</sub> over the WHTC. It was verified that one of the main reasons for the discrepancy between the requested and actual tailpipe NO<sub>x</sub> levels is due to the fact that the controller is switched on and off many times over the WHTC, since it is activated only when the required BMEP is higher than 0.5 bar. In particular, it resulted in engine operating at lower loads than 0.5 bar for a non-negligible part of the cycle, especially in the time instants before  $t = 1300$  s.

It was also verified that the average SCR system mean efficiency is very similar over the different simulations, and therefore the target offsets of tailpipe NO<sub>x</sub> emissions are met basically through target offsets of the engine-out NO<sub>x</sub> levels, which are achieved by means of the action of the combustion controller. In fact, as can be seen in Table 6, the percentage differences in the simulated tailpipe NO<sub>x</sub> levels are of the same order of magnitude as those of the simulated engine-out NO<sub>x</sub> levels.

It should be noted that in case that the efficiency of the SCR device deteriorates significantly (e.g., in cold conditions), the tailpipe NO<sub>x</sub> controller would set a very low level for the engine-out NO<sub>x</sub> target for the combustion controller through Equation (7), and

this could be effective in reducing tailpipe NO<sub>x</sub> emissions as much as possible until the SCR light-off is reached.

Figure 13 shows a comparison of the main results obtained in the simulation of the WHTC with the online strategy, offline strategy (with  $\beta = 1$ ), and baseline point, at roughly constant tailpipe NO<sub>x</sub> levels around 0.6 g/kWh.

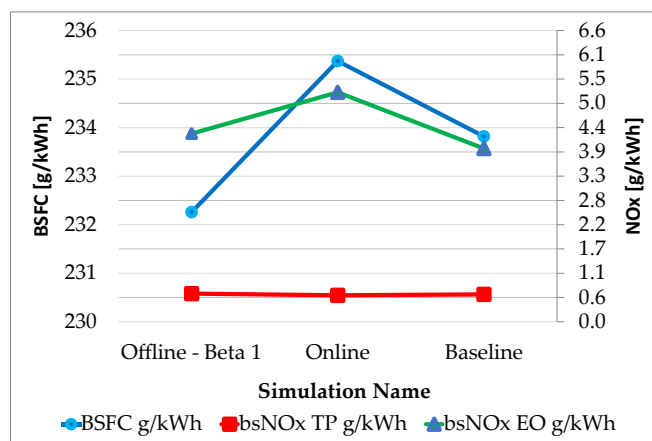


**Figure 13.** Comparison of the results obtained in the simulation of the WHTC with the online calibration strategy, offline calibration strategy with  $\beta = 1$  and baseline point, at roughly constant tailpipe NO<sub>x</sub> levels.

As previously noted, the best results are obtained using the offline strategy (with  $\beta = 1$ ), since this strategy allows to reduce BSFC with respect to the base calibration at roughly constant tailpipe NO<sub>x</sub> levels and AdBlue consumption.

The performance of the two strategies has also been compared by plotting, in Figure 14, the BSFC (Figure 14a), tailpipe bsNO<sub>x</sub> (Figure 14b), and bsAdBlue consumption (Figure 14c) as a function of the mean value of the engine-out NO<sub>x</sub> multiplier that was selected over the WHTC. With reference to the offline strategy, the relation between the chosen value of  $\beta$  and the resulting mean value of 'NO<sub>x</sub>\_EO\_Mult' is also shown in Figure 14d. It will be shown later that this trend is very useful for the practical application of the proposed method.

It is interesting to note in the figure that the two strategies lead to remarkably different values of the mean engine-out NO<sub>x</sub> multiplier over the WHTC. In particular, the offline strategy tends to adopt, on average, lower values of the 'NO<sub>x</sub>\_EO\_Mult', while the online strategy tends to select much higher values. Therefore, as can be seen in Figure 14b, both approaches have the potential to reduce tailpipe NO<sub>x</sub> emissions with respect to the baseline case, but this is realized by adopting different mean values of 'NO<sub>x</sub>\_EO\_Mult'. Also, the BSFC curves (Figure 14a) are remarkably different. For example, the BSFC obtained with the offline strategy when the average 'NO<sub>x</sub>\_EO\_Mult' is around 0.8 (i.e., 233 g/kWh) is much lower than that obtained with the online strategy at equal value of NO<sub>x</sub>\_EO\_Mult = 0.8 (i.e., 241 g/kWh). This suggests that the behavior of the two controllers over the WHTC, in terms of the instantaneous values of 'NO<sub>x</sub>\_EO\_Mult' which are set for the combustion controller, is expected to be very different, even when the mean value of this parameter is similar. This will be investigated and verified in the next paragraphs. The different behavior of the two strategies can be justified considering the intrinsic difference between the two methods: in the offline strategy, the 'NO<sub>x</sub>\_EO\_Mult' value is defined by a static lookup table, which derives from the objective function minimization, while in the online strategy 'NO<sub>x</sub>\_EO\_Mult' is evaluated at each time instant on the basis of the SCR efficiency. Concerning Figure 14c, it can be seen that the curves of the offline and online strategies are quite aligned, while Figure 14d shows how, in the offline strategy, the selection of higher  $\beta$  values (i.e., the selection of a more BSFC-oriented optimization) leads to higher average values of the mean 'NO<sub>x</sub>\_EO\_Mult', i.e., to the request of higher engine-out NO<sub>x</sub> levels.

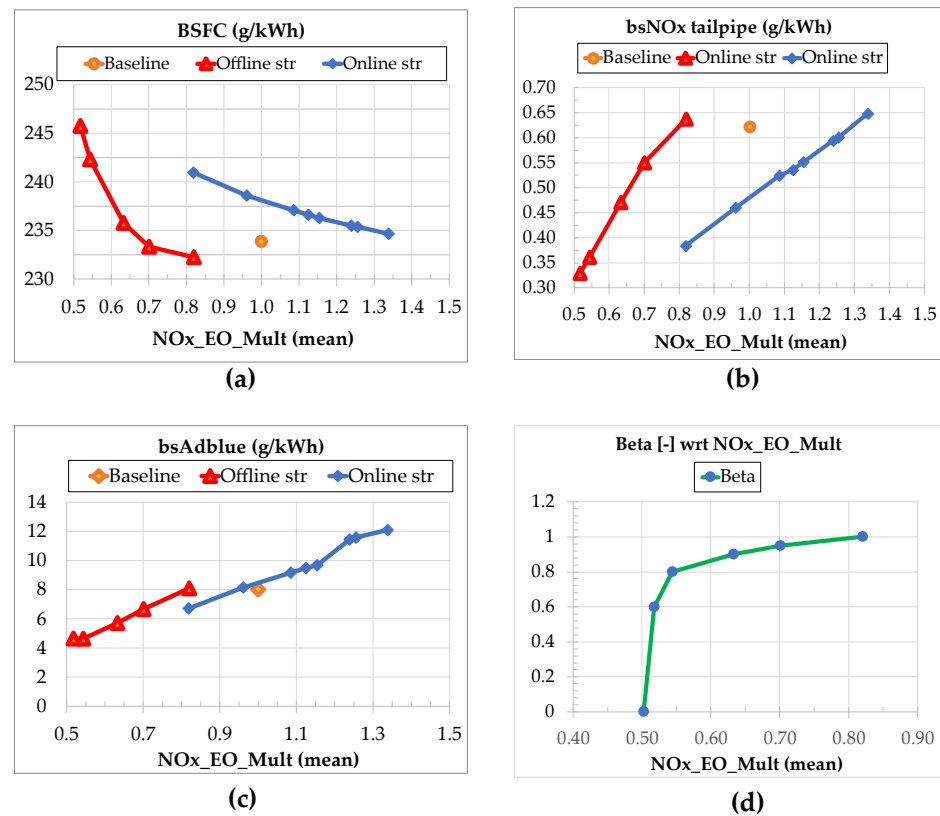


**Figure 14.** Values of BSFC (a), bsNOx tailpipe (b), and bsAdBlue consumption (c) as a function of ' $NOx\_EO\_Mult$ ', obtained with the offline and online calibration strategies, as well as for the baseline point. The relation between the chosen  $\beta$  and the mean  $NOx\_EO\_Mult$  identified by the offline calibration strategy is also shown in (d).

In a possible real-world application scenario of the proposed methods, one could define the best calibration in terms of BSFC and AdBlue consumption by means of offline strategy over the entire driving mission, and use the online strategy as an auxiliary algorithm to dynamically adjust the calibration parameters especially in critical conditions, such as during cold start when the ATS efficiency is low. In the latter condition, the online strategy is expected to set very low values of ' $NOx\_EO\_Mult$ ' (i.e., 0.5), which would lead to a retarded injection that limits the engine-out NOx levels to the minimum allowable values, and at the same time increases exhaust gas temperatures, with consequent benefits in terms of ATS light-off time, at the expense of a penalization in terms of BSFC. Moreover, as previously stated, the online strategy could be further refined, taking into account possible limits in terms of BSFC penalization or AdBlue consumption, for the definition of optimal tailpipe NOx targets.

The following figures present some details of the simulations of the WHTC. In particular, Figure 15 shows the trends, over the WHTC, of the NOx Multiplier (Figure 15a), tailpipe and engine-out cumulative NOx mass (Figure 15b) and fuel consumption (Figure 15c), for the three considered approaches (i.e., baseline, offline calibration strategy, online calibration strategy) which are tuned to give roughly the same integral tailpipe NOx levels (i.e., the calibration sets of Figure 13).

It can be seen that the offline strategy leads to a less aggressive selection of the NOx multiplier, compared with the online strategy, which often sets NOx multiplier values equal to the upper boundary of 1.5. This choice is made whenever the efficiency of the SCR is near to 1, a condition for which a very high engine-out NOx level is requested, which may lead to benefits in terms of BSFC due to a more anticipated injection timing.

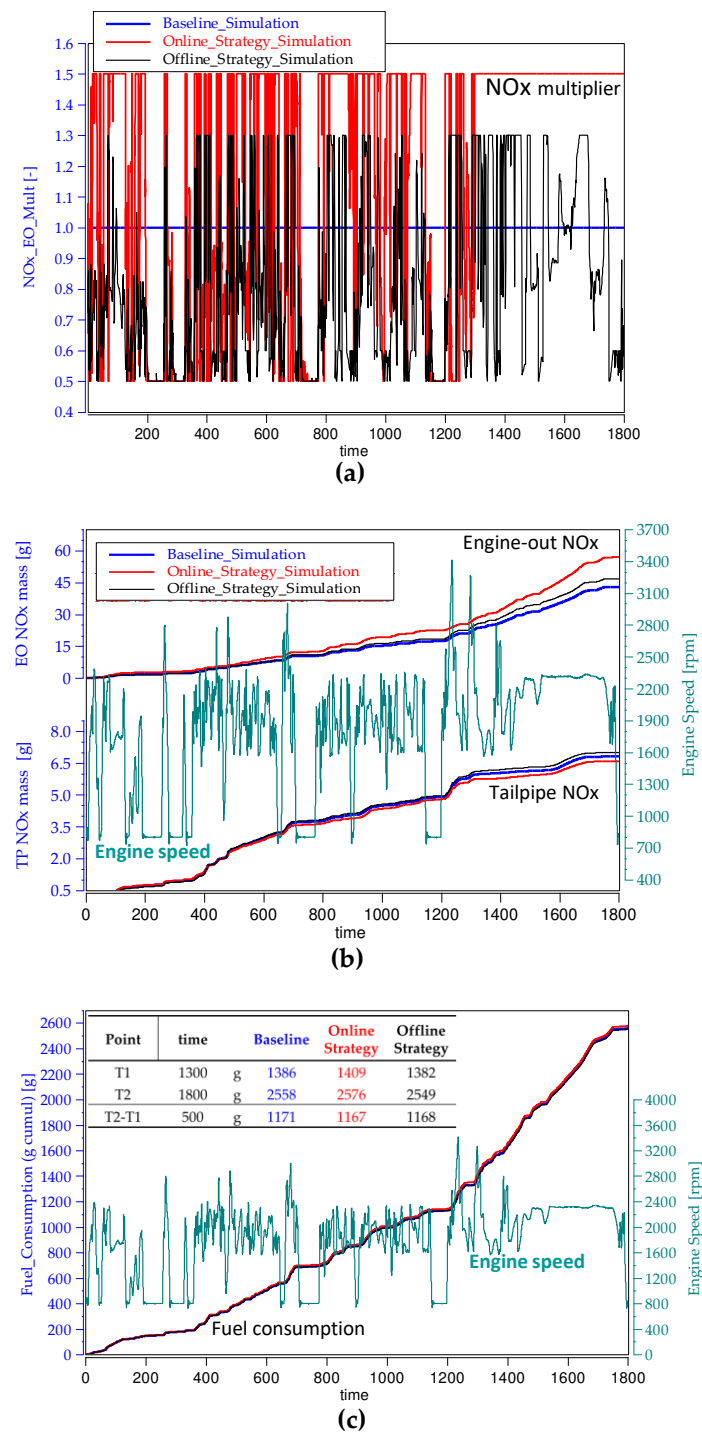


**Figure 15.** Comparison of the trends over the WHTC of the NO<sub>x</sub> Multiplier (a), tailpipe NO<sub>x</sub> mass and engine-out cumulative NO<sub>x</sub> mass (b), and fuel consumption (c) for the three considered approaches (i.e., baseline, offline strategy, online strategy) which are tuned to give roughly the same integral tailpipe NO<sub>x</sub> levels. The table in Figure 15c reports the consumed fuel in points T1 ( $t = 1300$  s) and T2 ( $t = 1800$  s) as well as their difference.

The use of the tailpipe NO<sub>x</sub> controller, which is based on the SCR's instantaneous efficiency value, leads to a selection of the highest engine-out NO<sub>x</sub> levels, especially at higher load conditions in the second part of the WHTC ( $t > 1300$  s). It can be seen in Figure 15c that this results in a slight amount of fuel saving with respect to the other cases, which however is not sufficient to compensate for the higher fuel consumption

which occurs in the first part of the cycle, over which the behavior of the online strategy is not optimal.

#### 4.2. Example of Application of the Offline Strategy

This section reports a practical example of application of the offline strategy, exploiting the results reported in Figure 14 and considering two possible scenarios:

- Scenario A: the target is to achieve a cumulative tailpipe NOx emission equal to 0.4 g/kWh over the WHTC.
- Scenario B: the target is to achieve the lowest possible BSFC over the WHTC.
- Concerning the first scenario, the procedure is shown in Figure 16, which reports the tailpipe bsNOx emissions (Figure 16a) and  $\beta$  (Figure 16b) as a function of the mean engine-out NOx multiplier over the WHTC.

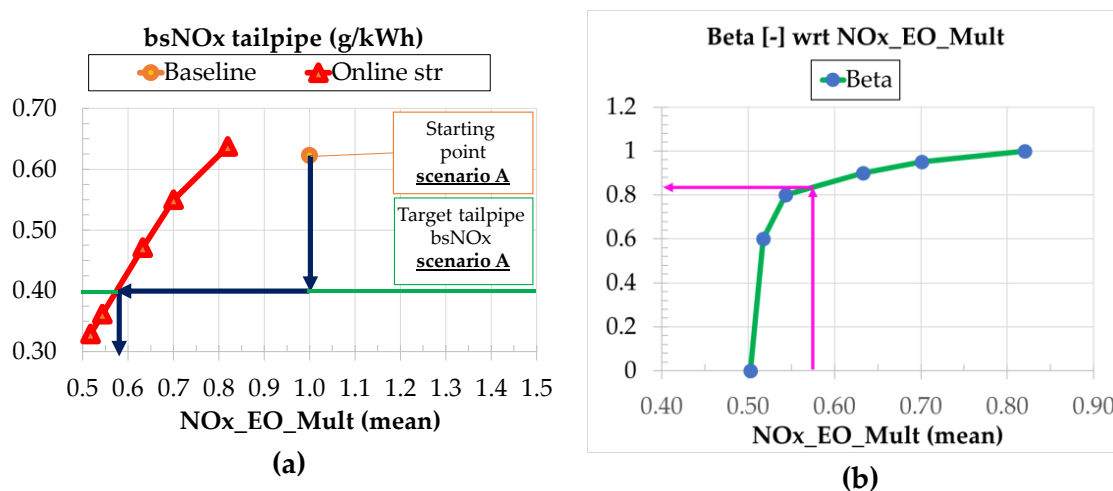


**Figure 16.** Offline calibration strategy: tailpipe bsNOx emissions (a) and  $\beta$  (b) as a function of the mean engine-out NOx multiplier over the WHTC.

The baseline point is represented with the orange circle in Figure 16a. The goal is to reduce tailpipe NOx emissions to 0.4 g/kWh starting from an initial level around 0.6 g/kWh. To achieve this, a mean value of  $NOx\_EO\_Mult = 0.58$  should be obtained over the WHTC cycle, and this can be achieved by setting a value of  $\beta = 0.84$  in the offline strategy (see Figure 16b).

The starting point and final point of Scenario A are compared in Table 7.

**Table 7.** Comparison of the baseline point and final point of Scenario A.

Mean $NOx\_EO\_Mult$	$\beta$	BSFC	bsNOx Engine-Out	bsNOx Tailpipe	bsAdBlue
-	-	g/kWh	g/kWh	g/kWh	g/kWh
Baseline	/	233.9	3.93	0.62	8
0.576	0.84	239.7	2.546	0.404	5.04
% differences		+2.5%	-35.2%	-34.8%	-37.0%

It can be seen in the table that the tailpipe bsNOx target of 0.4 g/kWh can be achieved at the expense of a worsening of BSFC of around 2.5% but with a reduction in AdBlue consumption of around 37%.

As far as Scenario B is concerned, the goal is to achieve the lowest possible BSFC over the WHTC. In order to achieve this, it is sufficient to impose  $\beta = 1$  in the offline strategy.

Table 8 reports a comparison of the baseline point and of the final point with minimum BSFC obtained in Scenario B.



**Table 8.** Comparison of the baseline point and final point of Scenario B.

529BMean NO <sub>x</sub> _EO_Mult	530Bβ	531BBSFC	532BbsNO <sub>x</sub> 533BEngine-out	534BbsNO <sub>x</sub> Tailpipe	535BbsAdblue
536B- 542B0.82 548BBaseline	537B- 543B1 549B/	538Bg/kWh 544B232.3 550B233.9	539Bg/kWh 545B4.26 551B3.93	540Bg/kWh 546B0.64 552B0.62	541Bg/kWh 547B8.1 553B8
554B% differences	555B	556B – 0.7%	557B8.4%	558B3.2%	559B1.3%

The offline strategy can optimize *BSFC* by up to 0.7% at virtually constant tailpipe bsNO<sub>x</sub> Tailpipe.

#### 4.3. Performance of the Online Strategy over a Mild Load Ramp

Finally, we investigated the performance of the online strategy also over a mild load ramp, in which BMEP was varied from 5 bar to 18 bar in around 20 s at constant engine speed equal to 2000 rpm. In these ramps, the engine warm-up was achieved after around 20 s, while the ATS warm-up was reached after about 80–90 s. Figure 17 presents the trends of the NO<sub>x</sub> Multiplier, SOI<sub>main</sub> correction with respect to the baseline value, and tailpipe NO<sub>x</sub> target/actual emissions for various cases:

- tailpipe NO<sub>x</sub> target from map;
- tailpipe NO<sub>x</sub> target from map, increase of 50%;
- tailpipe NO<sub>x</sub> target from map, decrease of 50%.

In the charts, positive corrections of SOI<sub>main</sub> correspond to more delayed injection timings with respect to the baseline case.

It can be seen that in case (a) the engine-out NO<sub>x</sub> multiplier is kept low during the increasing load ramp since SCR efficiency is still low. Instead, the NO<sub>x</sub> multiplier is set at 1.5 in the time interval between  $t = 85$  s and  $t = 95$  s, where the efficiency of the SCR is sufficiently high, and therefore higher engine-out NO<sub>x</sub> levels can be tolerated. In case (b), the NO<sub>x</sub> multiplier is set at 1.5 for most of the time, since high tailpipe NO<sub>x</sub> levels are requested (and, therefore, higher engine-out NO<sub>x</sub> emissions are set). Finally, in case (c), the NO<sub>x</sub> multiplier levels are lower than those of case (a), since lower tailpipe NO<sub>x</sub> emissions (and, therefore, lower engine-out levels) are requested.

Overall, the controller can be considered effective in responding to different tailpipe NO<sub>x</sub> requests.

#### 4.4. Final Considerations and Future Steps

Both developed strategies showed good potential for model-based calibration of tailpipe NO<sub>x</sub> emissions in diesel engines with ATS device. The adoption of the offline strategy allowed to obtain the best trade-off in terms of BSFC-tailpipe bsNO<sub>x</sub>, but this method requires more effort in terms of offline calculations for the definition of the different maps of the engine-out NO<sub>x</sub> multiplier. The online strategy, instead, is of immediate application, since it is based on a direct tailpipe NO<sub>x</sub> controller, which defines the engine-out NO<sub>x</sub> multiplier on the basis of the real-time value of the SCR efficiency, and does not require any offline calibration. Therefore, the online strategy can adapt the engine parameters in real-time, taking into account the thermal state of the ATS. Both strategies can potentially be implemented at the same time in the ECU, since they are computationally faster than alternative methods reported in the literature (e.g., DP-based, PMP-based, ECMS-based and MPC-based methods).

However, only a preliminary version of the algorithms has been presented in this study. Future steps will include the integration of additional controllers for the other pollutant emissions which are typically accounted for in diesel engines (e.g., soot, THC), in order to obtain a more comprehensive engine optimization tool, as well as the refinement of the online calibration strategy, in order to directly account for possible user-defined limits in

terms of BSFC and AdBlue penalizations when setting the engine-out NO<sub>x</sub> targets for the combustion controller.

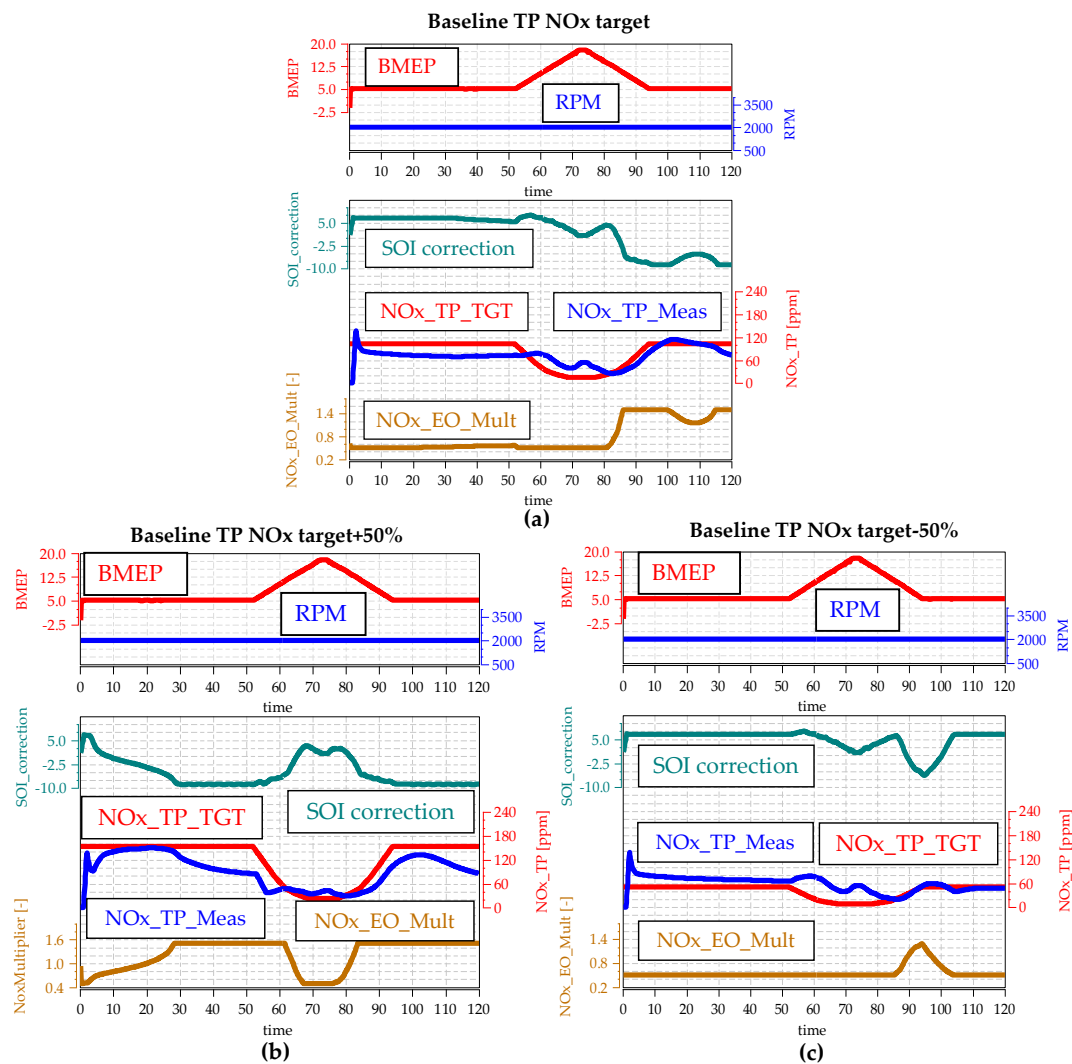


**Figure 17.** Trends of NO<sub>x</sub> Multiplier, SOI<sub>main</sub> correction with respect to the baseline value, and tailpipe NO<sub>x</sub> target/actual emissions, over a simulated mild load ramp at N = 2000 rpm, using the tailpipe NO<sub>x</sub> controller with nominal target (a), target increase of 50% (b), and target decrease of 50% (c).

## 5. Conclusions

In the present paper, two different strategies for the model-based calibration and control of tailpipe nitrogen oxide emissions were investigated for a light-duty 3.0 L diesel engine, equipped with after-treatment system (ATS). The engine was modeled in GT-SUITE environment, and a previously developed model-based combustion controller was integrated in the engine model, which adjusts injection timing and quantity to realize desired targets of engine-out NO<sub>x</sub> and BMEP. The first strategy, which is denoted as ‘offline strategy’, consisted of the minimization of an objective function ‘F’ that takes into account brake specific fuel consumption and AdBlue injection, with a weight factor  $\beta$  that can be chosen by the user. The second approach is an online strategy based on a direct model-based controller of tailpipe nitrogen oxide emissions, which exploits the real-time value of the SCR efficiency to define engine-out NO<sub>x</sub> emission targets for the combustion controller.

Both strategies were tested through Model-in-the-Loop (MiL) over a WHTC and a mild load ramp.

The main results can be summarized as follows:

- The offline strategy can achieve the best trade-off in terms of BSFC-tailpipe NO<sub>x</sub> emissions, leading to a BSFC reduction of about 2 g/kWh with respect to the baseline case over the WHTC at constant tailpipe NO<sub>x</sub> emissions.
- The online strategy, although showing a slight deterioration in terms of BSFC-tailpipe bsNO<sub>x</sub> trade-off over the WHTC simulation, has the potential to dynamically set the injection timing and injected fuel quantity depending on the actual efficiency of the SCR device. Therefore, in case that the efficiency of the SCR device deteriorates significantly (e.g., in cold conditions), the tailpipe NO<sub>x</sub> controller would set a very low level of the engine-out NO<sub>x</sub> target for the combustion controller, and this could be effective in reducing tailpipe NO<sub>x</sub> emissions as much as possible until the SCR light-off is reached. Moreover, this method requires less effort than the offline strategy since it does not need any offline calibration to be applied.
- The online strategy was also tested over a mild load ramp, in which BMEP was varied from 5 bar to 18 bar at N = 2000 rpm, and the tailpipe NO<sub>x</sub> target was varied of  $\pm 50\%$  with respect to the baseline one. Over the ramp, it demonstrated to be effective in following the instantaneous tailpipe NO<sub>x</sub> target requests, by dynamically setting different engine-out NO<sub>x</sub> targets for the combustion controller, on the basis of the actual SCR efficiency.
- Both strategies can potentially be implemented at the same time in the ECU, since they are computationally faster than alternative methods reported in the literature.

Future development steps will include the integration of additional controllers for the other pollutant emissions which are typically accounted for in diesel engines (e.g., soot, THC) as well as the refinement of the online calibration strategy in order to directly account for possible user-defined limits in terms of BSFC and AdBlue penalizations.

**Author Contributions:** The authors equally contributed to the deployment of the paper. Conceptualization, R.F., C.d.D. and S.d.; methodology, R.F., C.d.D. and S.d.; software, C.d.D.; formal analysis, R.F., C.d.D. and S.d.; data curation, R.F., C.d.D. and S.d.; writing—original draft preparation, R.F., C.d.D. and S.d.; writing—review and editing, R.F., C.d.D. and S.d.; supervision, R.F. and S.d. All authors have read and agreed to the published version of the manuscript.

**Funding:** This research received no external funding.

**Data Availability Statement:** Data sharing not applicable. No new data were created or analyzed in this study. Data sharing is not applicable to this article.

**Acknowledgments:** The authors would like to acknowledge AVL for the utilization of CAMEO 4 and CONCERTO 5 within the University Partnership Program.

**Conflicts of Interest:** The authors declare no conflict of interest.

## Abbreviations

AFM	accumulated fuel mass
ATS	after-treatment system
BMEP	Brake Mean Effective Pressure (bar)
BSFC	Brake Specific Fuel Consumption
CA	crank angle (deg)
DEF	Diesel Exhaust Fluid
DOC	Diesel Oxidation Catalyst
DP	Dynamic Programming
DPF	Diesel Particulate Filter
ECMS	Equivalent Consumption Minimization Strategy
ECU	Engine Control Unit
EGR	Exhaust Gas Recirculation
EU	European Union
EV	Electric Vehicle

EVO	Exhaust Valve Opening
FMEP	Friction Mean Effective Pressure (bar)
$H_{abs}$	Absolute air humidity
HEV	Hybrid Electric Vehicle
ICE	Internal Combustion Engine
IMEP	Indicated Mean Effective Pressure (bar)
IMEP360	net Indicated Mean Effective Pressure (bar)
IMEP720	gross Indicated Mean Effective Pressure (bar)
IMPERIUM	IMplementation of Powertrain Control for Economic and Clean Real driving emIssion and fuel ConsUMption
IVC	Intake Valve Closing
$m$	mass
$\dot{m}_{air}$	mass flow rate of fresh air
$\dot{m}_{EGR}$	mass flow rate of EGR
MFB50	crank angle at which 50% of the fuel mass fraction has burned (deg)
MiL	Model-in-the-Loop
MPC	model predictive control
N	engine rotational speed (1/min)
NFC	next firing cylinder
$O_2$	intake charge oxygen concentration (%)
$p$	pressure (bar)
$p_{cabin}$	test cell pressure (bar abs)
$p_{exh}$	exhaust manifold pressure (bar abs)
$p_f$	injection pressure (bar)
PFP	peak firing pressure
$p_{int}$	intake manifold pressure (bar abs)
PID	Proportional Integral Derivative
PMEP	Pumping Mean Effective Pressure (bar)
PMP	Pontryagin's minimum principle
$q$	injected fuel volume quantity ( $mm^3$ )
$Q_{ch}$	chemical heat release
$q_{f,inj}$	total injected fuel volume quantity per cycle/cylinder
$Q_{net}$	net heat release
RMSE	root mean square error
SCR	selective catalytic reduction
SOI	electric start of injection
$SOI_{main}$	electric start of injection of the main pulse
$t$	time (s)
$T$	temperature (K)
$T_{env}$	ambient temperature
$T_{int}$	intake manifold temperature
THC	total unburned hydrocarbons
$V$	volume
VGT	Variable Geometry Turbine
VPM	Virtual pressure model
WHTC	World Harmonized Transient Cycle

## Appendix A

This section reports the main validation results of the fast-running engine model developed in GT-SUITE [31] and the tuning results of the ATS system.

In particular, Figure A1a reports the predicted vs. experimental values of BMEP when setting the experimental injected fuel quantity as input in the model, Figure A1b reports the predicted vs. experimental values of engine-out NOx emissions, and Figure A1c reports the predicted vs. experimental values of air mass flow rate. All the quantities were calculated by adopting a computational step of 1 degree.

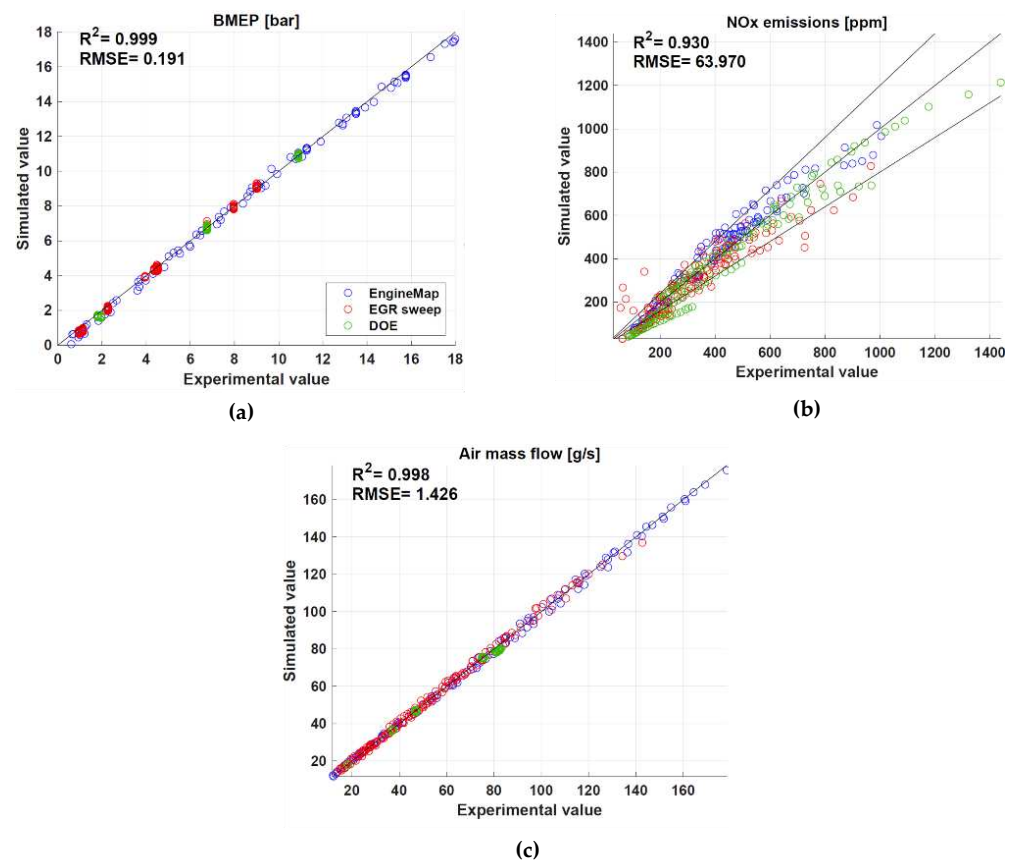


**Figure A1.** Predicted vs. experimental values of BMEP (a), engine-out NOx emissions (b), and air mass flow rate (c) for the fast-running engine model developed in GT-SUITE, using the tests reported in Figure 2. The results were taken from [31].

Concerning the tuning of the SCR device model, Figure A2 reports the simulated efficiency as a function of the parameter  $\alpha = \frac{n_{NH_3}}{n_{NOx}}$ , at 3500 full load engine point (which was taken as a reference for model calibration), in comparison with the expected trend (red dotted line), according to which the NOx conversion efficiency is proportional to the amount of reducing agent that is introduced in the exhaust flow [41] and reaches its maximum value for  $\alpha = 1$ . As can be seen, a good match has been obtained after model tuning.

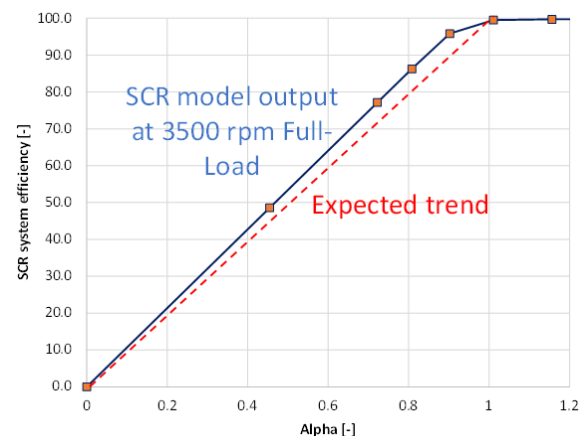


**Figure A2.** Simulated efficiency of the SCR device as a function of the  $\alpha$  parameter at 3500 full load engine point (which was taken as a reference for model calibration) in comparison with the ideal theoretical curve suggested in the GT-SUITE manual (red dotted line).

## References

1. Fit for 55: Zero CO<sub>2</sub> Emissions for New Cars and Vans in 2035. Available online: <https://www.europarl.europa.eu/news/en/press-room/20230210IPR74715/fit-for-55-zero-co2-emissions-for-new-cars-and-vans-in-2035> (accessed on 10 July 2023).
2. Opening Remarks by Executive Vice-President Timmermans at the Press Conference on the Revision of CO<sub>2</sub> Emission Standards for Heavy-Duty Vehicles. Available online: [https://ec.europa.eu/commission/presscorner/detail/en/speech\\_23\\_864](https://ec.europa.eu/commission/presscorner/detail/en/speech_23_864) (accessed on 10 July 2023).
3. In Win for Germany, EU Agrees to Exempt E-Fuels from 2035 Ban on New Sales of Combustion-Engine Cars. Available online: <https://www.euronews.com/my-europe/2023/03/28/in-win-for-germany-eu-agrees-to-exempt-e-fuels-from-2035-ban-on-new-sales-of-combustion-en> (accessed on 10 July 2023).
4. Range of Full Electric Vehicles. Available online: <https://ev-database.org/cheatsheet/range-electric-car> (accessed on 10 July 2023).
5. Liu, B.; Pantelidis, T.P.; Tam, S.; Chow, J.Y.J. An electric vehicle charging station access equilibrium model with M/D/C queueing. *Int. J. Sustain. Transp.* **2023**, *17*, 228–244. [CrossRef]
6. Ou, S. Estimate long-term impact on battery degradation by considering electric vehicle real-world end-use factors. *J. Power Sources* **2023**, *573*, 233133. [CrossRef]
7. Liang, S.; Zhu, B.; He, J.; He, S.; Ma, M. A pricing strategy for electric vehicle charging in residential areas considering the uncertainty of charging time and demand. *Comput. Commun.* **2023**, *199*, 153–167. [CrossRef]
8. Safarian, S. Environmental and energy impacts of battery electric and conventional vehicles: A study in Sweden under recycling scenarios. *Fuel Commun.* **2023**, *14*, 100083. [CrossRef]
9. Zhang, W.; Fang, X.; Sun, C. The alternative path for fossil oil: Electric vehicles or hydrogen fuel cell vehicles? *J. Environ. Manag.* **2023**, *341*, 118019. [CrossRef] [PubMed]
10. Xue, X.; Rutledge, J. Potentials of Electrical Assist and Variable Geometry Turbocharging System for Heavy-Duty Diesel Engine Downsizing. In *SAE Technical Paper Series*; SAE International: Warrendale, PN, USA, 2017. [CrossRef]
11. Mancarella, A.; Marelllo, O. Effect of Coolant Temperature on Performance and Emissions of a Compression Ignition Engine Running on Conventional Diesel and Hydrotreated Vegetable Oil (HVO). *Energies* **2023**, *16*, 144. [CrossRef]
12. D'Ambrosio, S.; Ferrari, A.; Mancarella, A.; Mancò, S.; Mittica, A. Comparison of the emissions, noise, and fuel consumption comparison of direct and indirect piezoelectric and solenoid injectors in a low-compression-ratio diesel engine. *Energies* **2019**, *12*, 4023. [CrossRef]
13. Al-Maidi, A.A.H.; Rodionov, Y.V.; Shchegolkov, A.V.; Nikitin, D.V.; Chernetsov, D.A.; Mikheev, N.V. Mathematical modeling of thermo-regulation of fuel in diesel engines. *Iraqi J. Agric. Sci.* **2018**, *49*, 70. [CrossRef]
14. Finesso, R.; Marelllo, O.; Spessa, E. Development of a pressure-based technique to control IMEP and MFB50 in a 3.0 L diesel engine. *Energy Procedia* **2018**, *148*, 424–430. [CrossRef]
15. Cococetta, F.; Finesso, R.; Hardy, G.; Marelllo, O.; Spessa, E. Implementation and Assessment of a Model-Based Controller of Torque and Nitrogen Oxide Emissions in an 11 L Heavy-Duty Diesel Engine. *Energies* **2019**, *12*, 4704. [CrossRef]
16. Finesso, R.; Hardy, G.; Marelllo, O.; Spessa, E.; Yang, Y. Model-Based Control of BMEP and NO<sub>x</sub> Emissions in a Euro VI 3.0 L Diesel Engine. *SAE Int. J. Engines* **2017**, *10*, 2288–2304. [CrossRef]
17. Nuss, E.; Wick, M.; Andert, J.; De Schutter, J.; Diehl, M.; Abel, D.; Albin, T. Nonlinear model predictive control of a discrete-cycle gasoline-controlled auto ignition engine model: Simulative analysis. *Int. J. Engine Res.* **2019**, *20*, 1025–1036. [CrossRef]
18. Van Dooren, S.; Amstutz, A.; Onder, C.H. A causal supervisory control strategy for optimal control of a heavy-duty Diesel engine with SCR aftertreatment. *Control Eng. Pract.* **2022**, *119*, 104982. [CrossRef]
19. Velmurugan, D.; McKelvey, T.; Lundberg, D. Supervisory Controller for a Light Duty Diesel Engine with an LNT-SCR After-Treatment System. In *SAE Technical Paper Series*; SAE International: Warrendale, PN, USA, 2018. [CrossRef]
20. Donkers, M.; Van Schijndel, J.; Heemels, W.; Willems, F. Optimal control for integrated emission management in diesel engines. *Control Eng. Pract.* **2017**, *61*, 206–216. [CrossRef]
21. Feru, E.; Murgovski, N.; Jager, B.; Willems, F. Supervisory Control of a Heavy-Duty Diesel Engine with an Electrified Waste Heat Recovery System. *Control Eng. Pract.* **2016**, *54*, 190–201. [CrossRef]
22. Chen, P.; Wang, J. Integrated Diesel Engine and Selective Catalytic Reduction System Active NO<sub>x</sub> Control for Fuel Economy Improvement. In Proceedings of the 2013 American Control Conference, Washington, DC, USA, 17–19 June 2013. [CrossRef]
23. Ma, Y.; Wang, J. Integrated Power Management and Aftertreatment System Control for Hybrid Electric Vehicles with Road Grade Preview. *IEEE Trans. Veh. Technol.* **2017**, *66*, 10935–10945. [CrossRef]
24. Westerlund, C.; Westerberg, B.; Odenbrand, I.; Egnell, R. Model Predictive Control of a Combined EGR/SCR HD Diesel Engine. In *SAE Technical Paper Series*; SAE International: Warrendale, PN, USA, 2010. [CrossRef]
25. Wassén, H.; Dahl, J.; Idelchi, A. Holistic diesel engine and exhaust after-treatment model predictive control. *IFAC-PapersOnLine* **2019**, *52*, 347–352. [CrossRef]
26. Karim, M.R.; Egardt, B.; Murgovski, N.; Gelso, E.R. Supervisory control for real-driving emission compliance of heavy-duty vehicles. *IFAC-PapersOnLine* **2018**, *51*, 460–466. [CrossRef]
27. Yamaguchi, T.; Aoyagi, Y.; Uchida, N.; Fukunaga, A.; Kobayashi, M.; Adachi, T.; Hashimoto, M. Fundamental Study of Waste Heat Recovery in the High Boosted 6-cylinder Heavy Duty Diesel Engine. *SAE Int. J. Mater. Manuf.* **2015**, *8*, 209–226. [CrossRef]
28. Samuel, J.; Ramesh, A. An Improved Physics-Based Combustion Modeling Approach for Control of Direct Injection Diesel Engines. *SAE Int. J. Engines* **2020**, *13*, 457–472. [CrossRef]

29. Ljung, L. Black-box models from input-output measurements. In Proceedings of the IMTC 2001, 18th IEEE Instrumentation and Measurement Technology Conference. Rediscovering Measurement in the Age of Informatics, Budapest, Hungary, 21–23 May 2001. [[CrossRef](#)]
30. Zhou, Q.; Lucchini, T.; D’Errico, G.; Novella, R.; Garcia Oliver, J.M.; Lu, X. CFD Modeling of Reacting Diesel Sprays with Primary Reference Fuel. *SAE Int. J. Adv. Curr. Prac. Mobil.* **2021**, *3*, 2433–2451. [[CrossRef](#)]
31. Ventura, L.; Finesso, R.; Malan, S.A. Development of a Model-Based Coordinated Air-Fuel Controller for a 3.0 dm<sup>3</sup> Diesel Engine and Its Assessment through Model-in-the-Loop. *Energies* **2023**, *16*, 907. [[CrossRef](#)]
32. Rakopoulos, C.; Giakoumis, E. Review of Thermodynamic Diesel Engine Simulations under Transient Operating Conditions. In *SAE Technical Paper Series*; SAE International: Warrendale, PN, USA, 2006. [[CrossRef](#)]
33. Feng, Y.; Wang, H.; Gao, R.; Zhu, Y. A Zero-Dimensional Mixing Controlled Combustion Model for Real Time Performance Simulation of Marine Two-Stroke Diesel Engines. *Energies* **2019**, *12*, 2000. [[CrossRef](#)]
34. Asprión, J.; Chinellato, O.; Guzzella, L. A fast and accurate physics-based model for the NO<sub>x</sub> emissions of Diesel engines. *Appl. Energy* **2013**, *103*, 221–233. [[CrossRef](#)]
35. Can, Ö.; Baklacioglu, T.; Öztürk, E.; Turan, O. Artificial neural networks modeling of combustion parameters for a diesel engine fueled with biodiesel fuel. *Energy* **2022**, *247*, 123473. [[CrossRef](#)]
36. Ventura, L.; Malan, S.A. Recurrent Neural Network to Estimate Intake Manifold O<sub>2</sub> Concentration in a Diesel Engine. In Proceedings of the 20th International Conference on Control, Automation and Systems, ICCAS 2020, Busan, Republic of Korea, 13–16 October 2020. [[CrossRef](#)]
37. Warey, A.; Gao, J.; Grover, R. Prediction of Engine-Out Emissions Using Deep Convolutional Neural Networks. *SAE Int. J. Adv. Curr. Prac. Mobil.* **2021**, *3*, 2863–2871. [[CrossRef](#)]
38. Finesso, R.; Hardy, G.; Maino, C.; Marelli, O.; Spessa, E. A New Control-Oriented Semi-Empirical Approach to Predict Engine-Out NO<sub>x</sub> Emissions in a Euro VI 3.0 L Diesel Engine. *Energies* **2017**, *10*, 1978. [[CrossRef](#)]
39. Miwa, J.T. Control of NO/NO<sub>2</sub> Ratio to Improve SCR Efficiency for Treating Engine Exhaust Using Bypass Oxidation Catalyst. U.S. Patent Application 8,420,036, B1, 16 April 2013.
40. SAE J1088\_201303; Test Procedure for the Measurement of Gaseous Exhaust Emissions from Small Utility Engines, Recommended Practice. SAE International: Warrendale, PN, USA, 2013.
41. Brzeżański, M.; Sala, R. The influence of AdBlue dosage on the process of selective catalytic reduction of nitrogen oxides. *Combust. Engines* **2013**, *154*, 1032–1037.

**Disclaimer/Publisher’s Note:** The statements, opinions and data contained in all publications are solely those of the individual author(s) and contributor(s) and not of MDPI and/or the editor(s). MDPI and/or the editor(s) disclaim responsibility for any injury to people or property resulting from any ideas, methods, instructions or products referred to in the content.